Journal Pre-proof



NEK2 and *PLK1* in pancreatic cancer cells induce endoplasmic reticulum stress-mediated dysfunction in beta cells under pancreatic cancer-associated diabetes mellitus

Jianyao Lou, Ze Zhang, Zengyu Feng, Haocheng Yu, Yuheng Tu, Jiali Gong, Yongji Sun, Meihua Shangguan, Kaiyue Pu, Ning Wang, Kaili Cai, Changming Lv, Xiawei Li, Xiaoping Liu, Yulian Wu

PII: S3117-3977(26)00069-3

DOI: https://doi.org/10.1016/j.tmed.2026.100068

Reference: TMED100068

To appear in: *TransMed*

Received date: 4 October 2026
Revised date: 9 November 2026
Accepted date: 12 November 2026

Please cite this article as: Jianyao Lou, Ze Zhang, Zengyu Feng, Haocheng Yu, Yuheng Tu, Jiali Gong, Yongji Sun, Meihua Shangguan, Kaiyue Pu, Ning Wang, Kaili Cai, Changming Lv, Xiawei Li, Xiaoping Liu and Yulian Wu, *NEK2* and *PLK1* in pancreatic cancer cells induce endoplasmic reticulum stress-mediated dysfunction in beta cells under pancreatic cancer-associated diabetes mellitus, *TransMed,* (2026) doi:https://doi.org/10.1016/j.tmed.2026.100068

This is a PDF of an article that has undergone enhancements after acceptance, such as the addition of a cover page and metadata, and formatting for readability. This version will undergo additional copyediting, typesetting and review before it is published in its final form. As such, this version is no longer the Accepted Manuscript, but it is not yet the definitive Version of Record; we are providing this early version to give early visibility of the article. Please note that Elsevier's sharing policy for the Published Journal Article applies to this version, see: https://www.elsevier.com/about/policies-and-standards/sharing#4-published-journal-article. Please also note that, during the production process, errors may be discovered which could affect the content, and all legal disclaimers that apply to the journal pertain.

© 2026 Publishing services by Elsevier B.V. on behalf of KeAi Communications Co. Ltd.

NEK2 and *PLK1* in pancreatic cancer cells induce endoplasmic reticulum stress-mediated dysfunction in beta cells under pancreatic cancer-associated diabetes mellitus

Jianyao Lou[a,b,c1], Ze Zhang[d,g1], Zengyu Feng[a,b,c1], Haocheng Yu[a,b,c], Yuheng Tu[a,b,c], Jiali Gong[a,b,c], Yongji Sun[a,b,c], Meihua Shangguan[a,b,c], Kaiyue Pu[a,b,c], Ning Wang[a,b,c], Kaili Cai[f], Changming Lv[f], Xiawei Li[a,b,c,e*], Xiaoping Liu[d*], Yulian Wu[a,b,c,f*]

[a] Department of General Surgery, Second Affiliated Hospital, Zhejiang University School of Medicine, Hangzhou 310000, Zhejiang, China

[b] Key Laboratory of Cancer Prevention and Intervention, China National Ministry of Education, Cancer Institute, Second Affiliated Hospital, Zhejiang University School of Medicine, Hangzhou 310000, Zhejiang, China

[c] Cancer Center, Zhejiang University, Hangzhou 310000, Zhejiang, China

[d] Key Laboratory of Systems Health Science of Zhejiang Province, School of Life Science, Hangzhou Institute for Advanced Study, University of Chinese Academy of Sciences, Hangzhou 310000, Zhejiang, China

[e] Harvard T.H. Chan School of Public Health, Harvard University, Boston 02115, MA, USA

[f] Department of General Surgery, Fourth Affiliated Hospital, Zhejiang University School of Medicine, Yiwu 322000, Zhejiang, China

[g] Department of Institute of Medical Artificial Intelligence, South China Hospital, Medical School, Shenzhen University, Shenzhen 518116, China

[1] These authors contributed equally to this work.

Journal Pre-proof

* Co-corresponding authors

Corresponding author:

Yulian Wu, M.D., Ph.D.

Department of General Surgery, Second Affiliated Hospital, Zhejiang University School of Medicine, Hangzhou 310000, Zhejiang, China.

Tel: +86-571-87784604 Fax: +86-571-87784604 E-mail: yulianwu@zju.edu.cn

Co-corresponding author:

Xiaoping Liu, Eng.D, Ph.D.

Key Laboratory of Systems Health Science of Zhejiang Province, School of Life Science, Hangzhou Institute for Advanced Study (HIAS), University of Chinese Academy of Sciences (UCAS), No.1 Xiangshan Branch, Hangzhou 310024, Zhejiang, China

Tel: +86-571-86080306 Fax: +86-571-86080306 E-mail: xpliu@ucas.ac.cn

Co-corresponding author:

Xiawei Li, M.D., MPH

Department of General Surgery, Second Affiliated Hospital, Zhejiang University School of Medicine, Hangzhou 310000, Zhejiang, China.

Tel: +86-571-87784604 Fax: +86-571-87784604 E-mail: xiaweili@hsph.harvard.edu

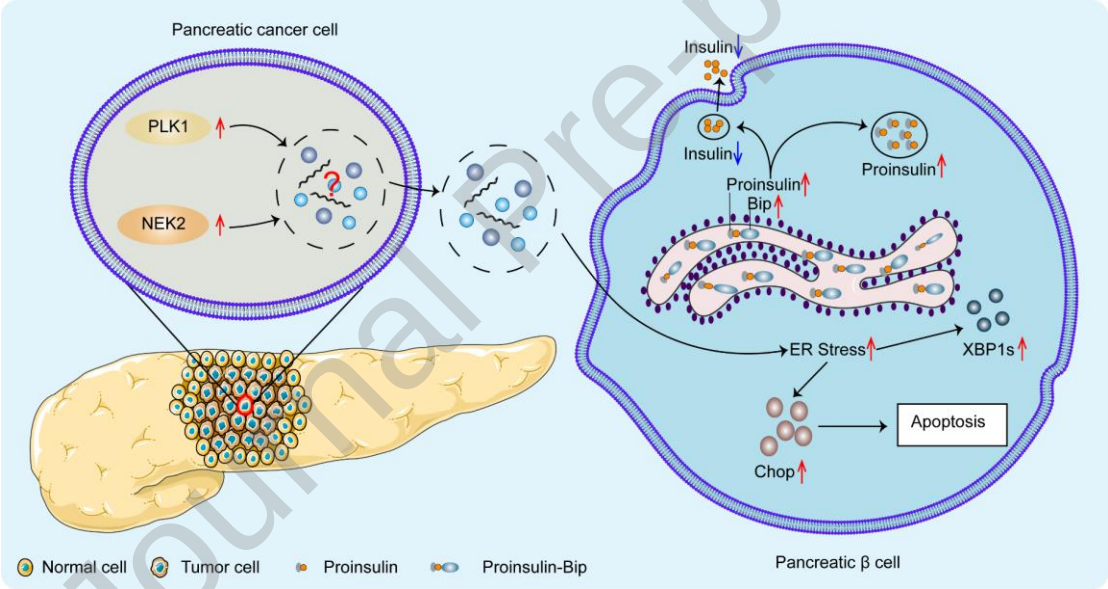
Key words: Pancreatic cancer-associated diabetes mellitus; Sample-specific network; PLK1; NEK2; Endoplasmic reticulum stress

Journal Pre-proof

Highlights

- NEK2 and PLK1 are driver genes of pancreatic cancer-associated diabetes (PaCDM).
- NEK2/PLK1 induce ER stress-mediated β-cell dysfunction in PaCDM.
- Silencing NEK2 or PLK1 alleviates glucose intolerance in mice.
- NEK2 and PLK1 act independently in pancreatic cancer cells.
- Downstream secreted molecules may aid early detection of PaC in new-onset diabetes.

Graphic abstract



Journal Pre-proof

Abstract

Pancreatic cancer-associated diabetes mellitus (PaCDM) mechanisms remain unclear, hindering early detection of pancreatic cancer (PaC) in patients with new-onset diabetes. Using sample-specific network analysis of PaC RNA-seq data and immunohistochemical validation, we identified *NEK2* and *PLK1* as potential driver genes upregulated in PaC, especially in cases with new-onset diabetes. Overexpression of NEK2 or PLK1 in PaC cells impaired β-cell function, reducing insulin secretion, insulin mRNA/protein, and β-cell viability independently. The NEK2 inhibitor Nek2-IN-5 and PLK1 inhibitor BI6727 reproduced the effects of NEK2 or PLK1 knockdown. Mechanistically, overexpression of NEK2 or PLK1 in PaC cells triggered endoplasmic reticulum (ER) stress, apoptosis, and proinsulin accumulation in β cells; these effects were reversed by the ER stress inhibitor RH01386, and the decreased insulin content was ER stress-dependent. *In vivo*, silencing NEK2 or PLK1 alleviated glucose intolerance and ER stress in mice with subcutaneous/orthotopic Panc02 tumors. Thus, NEK2 and PLK1 in PaC cells induce ER stress-mediated β-cell dysfunction in PaCDM, and their downstream molecules may serve as targets for early detection of PaC in patients with new-onset diabetes.

Journal Pre-proof

Introduction

The well-documented association between pancreatic cancer (PaC) and diabetes mellitus (DM) underscores the critical importance of early PaC detection in individuals with new-onset DM, typically defined as within three years of initial DM diagnosis. Epidemiological evidence indicates that, against a background population incidence of only 0.012%, approximately 1% of patients aged 50 or above with new-onset DM are diagnosed with PaC within three years, establishing new-onset DM as a significant warning sign of underlying pancreatic malignancy [1]. Furthermore, clinical studies reveal that up to 80% of PaC patients present with either impaired glucose tolerance or overt new-onset DM [2-4]. And the frequent resolution of hyperglycemia following pancreaticoduodenectomy in these patients strongly suggests that diabetes in this context is directly associated with the cancer, a condition now widely recognized as pancreatic cancer-associated DM (PaCDM) [5]. Notably, PaC is often at an early and resectable stage at the onset of PaCDM, providing a critical window of 5-29 months for early intervention and treatment [6].

However, distinguishing PaCDM from common type 2 DM (T2DM) within the broad population of new-onset DM remains a clinical challenge due to their overlapping symptomatology [7]. Accumulating evidence suggests that PaCDM arises primarily from impaired β-cell secretory function, in contrast to the peripheral insulin resistance that characterizes T2DM [8]. In recent years, several tumor-derived factors have been proposed to contribute to β-cell dysfunction in PaCDM, such as adrenomedullin [5, 7], vanin-1 (VNN1) [9, 10], microRNA-19a [11], and macrophage migration inhibitory factor [12]. Despite these advances, the molecular pathogenesis of PaCDM remains incompletely elucidated, owing to scarce transcriptomic resources from well-defined PaCDM cohorts, a historical reliance on non-tissue-specific analyses, and the limited capacity of

conventional bioinformatics methods to resolve the complex gene-regulatory networks involved.

The sample-specific network (SSN) method, developed by Liu et al., provides a powerful framework for reconstructing functional gene networks at the individual sample level [13]. In contrast to conventional approaches that rely on large cohorts to infer generalized interaction patterns, SSN employs a mathematical model to detect differential gene-gene correlations between a single sample and a reference group, thereby capturing sample-specific alterations in gene regulatory relationships. By constructing an individual-specific network for each sample, SSN enables high-resolution delineation of the heterogeneous molecular mechanisms underlying complex diseases. Its utility was demonstrated in a study of drug-resistant and drug-sensitive lung cancer cell lines, where SSN identified distinct molecular networks driving the resistance phenotype using only two biological replicates per condition [13]. This capability to infer robust network topology from limited sequencing data makes SSN particularly suitable for investigating PaCDM pathogenesis, for which transcriptomic data from pancreatic tumor tissues of patients with documented diabetes status are currently scarce.

NIMA-related kinase 2 (NEK2) and Polo-like kinase 1 (PLK1) are serine/threonine kinases that are best known for their fundamental roles in mitosis and cell cycle progression. NEK2 regulates centrosome separation, microtubule organization, the spindle assembly checkpoint, and chromosome congression/segregation, whereas PLK1 controls centrosome maturation, mitotic entry, kinetochore-microtubule attachment, and cytokinesis [14, 15]. Both kinases are frequently overexpressed in human cancers and correlate with poor prognosis. In pancreatic cancer, NEK2 has been identified as a prognostic biomarker and promotes immune evasion by stabilizing PD-L1, while PLK1 supports tumor cell proliferation and chemoresistance, at least partly through

PI3K/AKT signaling; PLK1 inhibitors have also entered clinical evaluation for pancreatic ductal adenocarcinoma [14, 15]. Despite these advances, the contribution of NEK2 and PLK1 to PaCDM, especially β-cell dysfunction, remains largely unknown. Beyond the cell cycle, PLK1 is involved in the DNA damage response, autophagy, apoptosis, EMT, inflammatory signaling, and metabolic reprogramming, and NEK2 regulates PI3K-AKT, Wnt-β-catenin, MAPK-ERK, Hippo-YAP1, and NIK-NF-κB pathways, as well as mRNA splicing, p53, cilium disassembly, and immune escape [14, 15]. Although these pathways can crosstalk with endoplasmic reticulum (ER) stress and the unfolded protein response, direct evidence linking NEK2 or PLK1 to ER stress in other tumors or metabolic diseases remains scarce. Thus, whether NEK2 and PLK1 in PaC cells could induce ER stress-mediated β-cell impairment and thereby contribute to new-onset diabetes represents an important unresolved question.

In this study, we applied the SSN method to construct a functional gene network for PaCDM. Further analysis identified *NEK2* and *PLK1* as potential driver genes through rigorous stability analysis and experimental validation using glucose-stimulated insulin secretion (GSIS) assays. We found that both genes were significantly upregulated in pancreatic tumor tissues, particularly in patients with PaCDM. Subsequent *in vitro* experiments demonstrated that overexpression of *NEK2* or *PLK1* in PaC cells led to impaired insulin secretion, decreased insulin mRNA and protein levels, and reduced viability in β cells. Furthermore, such overexpression induced ER stress in β cells, an effect that was attenuated by the ER stress inhibitor RH01386. The observed ER stress was correlated with diminished insulin protein content, and this decrease was similarly rescued by RH01386 treatment. *In vivo*, silencing *NEK2* or *PLK1* in PaC cells alleviated PaC cell-induced glucose intolerance in mouse models. Collectively, our findings establish *NEK2* and *PLK1* as driver genes in PaCDM,

providing mechanistic insights into its pathogenesis and suggesting potential avenues for the early detection of pancreatic cancer.

Journal Pre-proof

Results

The functional gene network of PaCDM is constructed by SSN theory

To construct SSNs, 57 paraneoplastic adjacent non-cancerous pancreatic tissue samples from CPTAC-3 (n=46) and ORGANOID-PANCREATIC (n=11) were used as reference samples. After a common $\log_2(x + 1)$ transformation and gene identifier harmonization, a reference network was constructed using pairwise Pearson correlation coefficients (*PCC*s; Fig. 1A). Each of the eight pancreatic cancer samples (four samples of pancreatic cancer without diabetes (PaC group) and four samples of pancreatic cancer with diabetes (PaCDM group); S'_d and S''_d) was then individually added to the reference set to generate perturbed networks (Fig. 1B), and differential edges were defined as $\Delta PCC = PCC_{n+1} - PCC_n$ and assessed by Z-test ($p < 0.01$), yielding eight individual-specific networks (Fig. 1C). Intersecting the edges across these networks retained 102,710 shared differential edges, and a paired-samples t-test ($p < 0.0001$) identified 975 edges that differed significantly between PaC and PaCDM SSNs. These 975 edges were used to construct a functional gene network representing PaCDM pathogenesis (Fig. S1A). From this network, we extracted a subnetwork comprising the top 10 candidate genes ranked by their degree centrality (Fig. 2A).

These candidate genes and their respective degree values were as follows: WD repeat domain 31 (*WDR31*, 45), Mitochondrial ribosomal protein L11 (*MRPL11*, 38), Raf-1 proto-oncogene serine/threonine kinase (*RAF1*, 24), DEAD-box helicase 20 (*DDX20*, 20), Proteasome 26S subunit ATPase 1 (*PSMC1*, 20), Kinesin family member 14 (*KIF14*, 14), Polo like kinase 1 (*PLK1*, 14), Ribosomal protein S24 (*RPS24*, 13), NIMA related kinase 2 (*NEK2*, 11), and Protein kinase cAMP-dependent type I regulatory subunit beta (*PRKAR1B*, 11). Notably, none of the 10 candidate genes showed significant differential expression at the mRNA level, with fold-change values of PaCDM

versus PaC ranging between 0.66 and 1.5 (Fig. 2B).

NEK2 and *PLK1* are potential driver genes of PaCDM

To assess the reliability and gain further insights into the functionality of the top 10 candidate genes and corresponding first-order genes set, we performed KEGG pathway analysis. The results indicated a preliminary association between these candidate genes and the regulation of the insulin signaling pathway (Fig. S1B).

To minimize bias from arbitrary threshold selection, we conducted a stability analysis by systematically varying the *p*-value threshold (from 0.05 to 0.0001) in the Paired-Samples T-test used to identify significant edges. At $p < 0.05$, 6,408 edges showed significant differences, while a more stringent threshold ($p < 0.0001$) retained 975 edges. The impact of this edge reduction on the degree centrality of the 10 candidate genes is visualized in a box plot (Fig. 2C). We further calculated the median and interquartile range (IQR) of degree values for these 10 candidate genes across thresholds (Fig. 2D). Among the genes, *KIF14*, *RPS24* and *PRKAR1B* showed a median and IQR of 0, indicating higher computational randomness in their values within the network when different thresholds were applied. In contrast, the remaining 7 genes exhibited increasing IQR values, reflecting varying degrees of robustness. Among them, *NEK2* (IQR = 3) and *PLK1* (IQR = 5) demonstrated the highest stability, with both IQRs remaining below 10, suggesting their consistent importance in the network under changing statistical stringency and supporting their roles as potential driver genes in PaCDM.

To functionally assess the 10 candidate genes, GSIS, a classic *in vitro* assay for evaluating external factor effects on pancreatic β cells insulin secretion [10, 16], is extensively employed in studies investigating pancreatic cancer-induced β-cell dysfunction, with the PANC-1 cell line routinely

utilized to assess candidate genes through targeted knockdown protocols [5, 7]. Each candidate gene was silenced using two independent short hairpin RNAs (shRNAs) (Figs. S2A, B and S2E-L), and conditioned medium (CM) was collected from PANC-1 cells pretreated with sh-NC (CM-sh-NC) and following shRNAs (sh-NEK2#2 (CM-sh-NEK2#2), sh-PLK1#1 (CM-sh-PLK1#1), sh-WDR31#1 (CM-sh-WDR31#1), sh-MRPL11#1 (CM-sh-MRPL11#1), sh-RAF1#1 (CM-sh-RAF1#1), sh-DDX20#1 (CM-sh-DDX20#1), sh-PSMC1#1 (CM-sh-PSMC1#1), sh-KIF14#2 (CM-sh-KIF14#2), sh-RPS24#2 (CM-sh-RPS24#2), sh-PRKAR1B#2 (CM-sh-PRKAR1B#2)). Then MIN6 cells, which are widely used as β cell model, were treated with control medium (fetal bovine serum (FBS)-free fresh RPMI-1640) and above CM. For all *in vitro* experiments, control (Ctrl) refers to MIN6 cells treated with control medium, and CM-sh-NC served as the positive control. The reversal rate (%) was calculated as [Insulin (CM-sh-candidate gene) - Insulin (CM-sh-NC)] / [Insulin (Ctrl) - Insulin (CM-sh-NC)] × 100, where Insulin (CM-sh-candidate gene), Insulin (CM-sh-NC), and Insulin (Ctrl) denote the mean insulin concentrations in MIN6 cells treated with CM from candidate gene-knockdown PANC-1 cells, CM from sh-NC PANC-1 cells, and control MIN6 cells, measured by GSIS, respectively. GSIS assay revealed that only CM from *NEK2*- or *PLK1*-silenced PANC-1 cells significantly restored insulin secretion in MIN6 cells under both low- and high-glucose conditions compared to the CM-sh-NC (Figs. 2E, F and Figs. S2C, D). In contrast, CM from PANC-1 cells silenced for the other 8 candidate genes generally failed to alleviate the PANC-1 cells-induced suppression of insulin secretion in MIN6 cells (Figs. S2M-T). Minor exceptions included CM from *DDX20*- and *PSMC1*-silenced cells under low glucose, and *RAF1*-silenced cells under high glucose, which showed significant mitigation. Conversely, *RPS24* silencing in PANC-1 cells exacerbated insulin secretion impairment under high-glucose conditions.

Based on the convergence of SSN method, stability analysis, and functional GSIS validation, we identified *NEK2* and *PLK1* as potential driver genes in PaCDM pathogenesis.

NEK2 and PLK1 are upregulated in pancreatic cancer and are associated with the onset of PaCDM independently.

A total of 163 patients were included, comprising 108 patients in the PaC group and 55 patients in the PaCDM group. The composition of this cohort and the patient inclusion/exclusion process are summarized in a STROBE-style flow diagram (Fig. S1C). The baseline clinical and pathological characteristics are summarized in Table 1. Age, gender, body mass index (BMI), tumor diameter, TNM stage, T/N/M stage, vascular invasion, perineural invasion, adipose tissue invasion, and WHO differentiation grade were comparable between the two groups (all $p > 0.05$). These variables were therefore included as covariates in the adjusted analyses where appropriate.

To elucidate the association between NEK2/PLK1 expression levels in pancreatic cancer and the onset of PaCDM clinically, we performed immunohistochemical (IHC) staining for NEK2 and PLK1 in 15 paired pancreatic tumor and adjacent paraneoplastic tissues (Figs. 3A, B). Both proteins showed significantly higher expression in tumor tissues compared with their corresponding adjacent paraneoplastic tissues (Tables S4 and S5). We further assessed the relationship between NEK2/PLK1 expression and PaCDM in an independent cohort of 108 PaC and 55 PaCDM patients. Among the cohort, 36 samples were excluded from the correlation analysis between NEK2/PLK1 and insulin protein levels due to the absence of detectable pancreatic islet tissue in their sections for insulin IHC scoring. NEK2 staining intensity was significantly stronger in the PaCDM group than in the PaC group (Figs. 3C, D), and stronger NEK2 staining intensity was associated with weaker staining intensity of Insulin (Figs. 3C, E and Fig. S3A). Similarly, PLK1 expression was higher in

PaCDM tissues (Figs. 3F, G) and negatively correlated with insulin expression (Figs. 3F, H and Fig. S3B). These results confirmed the clinical relevance of NEK2 and PLK1 upregulation in PaCDM development.

To delineate the cellular-level association between NEK2/PLK1 expression dynamics and PaCDM pathogenesis, we analyzed their expression in human normal pancreatic ductal epithelial cells (HPDE6) and three orthotopic pancreatic cancer cell lines (BxPC-3, MIA PaCa-2, PANC-1), selected to reflect the genetic heterogeneity of early-stage PaC. CM from these cell lines was used to treat MIN6 cells (CM-HPDE6, CM-BxPC-3, CM-MIA PaCa-2, CM-PANC-1); GSIS and intracellular insulin content were assessed after 48 hours, while cell viability was measured at 72 hours. At the mRNA level, both *NEK2* and *PLK1* were significantly upregulated in PANC-1 cells, but not in BxPC-3 or MIA PaCa-2 cells, compared to HPDE6 cells (Figs. S3C, D). Protein analysis confirmed elevated NEK2 expression only in PANC-1 cells (Fig. S3C), whereas PLK1 was overexpressed in all three PaC lines, most prominently in PANC-1 cells (Fig. S3D). Functional assays revealed that CM-HPDE6 had no obvious detrimental effect on MIN6 cells, with insulin secretion under both low- and high-glucose conditions, intracellular insulin content, and cell viability all comparable to those of cells treated with fresh serum-free RPMI-1640 (Figs. 3I-L). In contrast, only CM from PANC-1 cells, which highly express both NEK2 and PLK1, significantly suppressed insulin secretion in MIN6 cells under both low- and high-glucose conditions (Figs. 3I, J), reduced intracellular insulin content (Fig. 3K), and impaired MIN6 cell viability (Fig. 3L). Moreover, this inhibitory effect of CM-PANC-1 on insulin content in MIN6 cells exhibited both time-dependent, with respect to CM collection duration, and concentration-dependent characteristics (Figs. S3R-S). CM from BxPC-3 and MIA PaCa-2 cells, which express lower levels

of NEK2 and PLK1, had minimal effects on insulin secretion and content, though they still moderately reduced cell viability (Figs. 3I-L). Notably, the nearly identical responses induced by Ctrl and CM-HPDE6, together with the minimal effects of CM-BxPC-3 and CM-MIA PaCa-2 on insulin secretion and content, indicate that consumed nutrients, metabolic by-products, and other nonspecific medium-related factors made a negligible contribution to the beta-cell dysfunction induced by pancreatic cancer cell-derived CM. Accordingly, fresh serum-free RPMI-1640 was used directly as the reference control in the subsequent experiments of this study. These results suggested that PaC-induced β-cell dysfunction, which functionally recapitulate PaCDM pathogenesis, was closely associated with the baseline expression levels of NEK2 and PLK1. Based on these observations, we selected PANC-1 cells for subsequent knockdown experiments to assess functional rescue, and MIA PaCa-2 cells for overexpression studies to evaluate gain-of-function effects on β-cell impairment.

Then, we first confirmed efficient knockdown of NEK2 and PLK1 in PANC-1 cells using sh-NEK2#1/#2 and sh-PLK1#1 (Figs. S3E-G), and successful overexpression of NEK2 and PLK1 in MIA PaCa-2 cells using OE-NEK2 and OE-PLK1 (Fig. S3H). Neither gene significantly affected the expression of the other upon perturbation (Figs. S3E, H). Previous phosphoproteomic analyses of clinical samples suggested that phosphorylated NEK2 was undetectable in pancreatic cancer [17]. In line with this, modulating NEK2 expression did not alter PLK1 phosphorylation in either PANC-1 or MIA PaCa-2 cells (Fig. S3I). Semi-endogenous Co-IP in MIA PaCa-2 cells overexpressing NEK2-HA or PLK1-Flag further showed that immunoprecipitation of either protein failed to co-precipitate the other, indicating that NEK2 and PLK1 do not physically interact in MIA PaCa-2 cells (Figs. S3J-K). Consistent with these findings, cell viability and apoptosis assays showed that under

standard DMEM conditions, PLK1 promoted pancreatic cancer cell viability, whereas NEK2 expression was not associated with viability (Figs. S3L-M). Under serum-free RPMI 1640 conditions used for CM collection, neither PLK1 nor NEK2 expression was significantly associated with cell viability (Figs. S3N-O), and apoptosis was not markedly affected by modulation of either protein under either culture condition (Figs. S3P-Q). Given that NEK2 and PLK1 are intracellular proteins that are not secreted, they are unlikely to directly mediate pancreatic cancer cell-induced MIN6 cell injury in the extracellular environment. We therefore hypothesized that secreted proteins downstream of NEK2 and PLK1 mediate this injury. To test this hypothesis, we performed secretome profiling in PANC-1 cells after NEK2 or PLK1 knockdown. Finally, data-independent acquisition mass spectrometry (DIA-MS)-based secretome profiling of CM from PANC-1 cells after NEK2 or PLK1 knockdown revealed extensive changes in secreted proteins, including both unique and shared downregulated proteins (Fig. S3T), with detailed lists provided in Figs. S3U, V. Therefore, within the framework of the present experimental design, rather than their effects on pancreatic cancer cell viability, the NEK2- or PLK1-induced alterations in intracellular signaling pathways in PaC cells were more likely to be the driving mechanism underlying PaC cell-mediated MIN6 cell impairment. Collectively, these results suggest that NEK2 and PLK1 function largely independently in PaC cells, although their downstream secretomes partially overlap; the precise interplay between their downstream secretory programs remains complex and warrants further investigation.

These findings indicate that NEK2 and PLK1 are upregulated in PaC and are associated with the onset of PaCDM independently.

NEK2 and PLK1 cause PaC cell-induced dysfunction of insulin

Journal Pre-proof

secretion and inhibition of cell viability in MIN6 cells.

To establish *NEK2* and *PLK1* as driver genes of PaC-induced β-cell impairment, we performed loss-of-function and gain-of-function studies using CM-based assays. CM was then collected from transfected cells and used to treat MIN6 cells. CM-sh-NC served as a positive control, while CM from OE-NC-transfected MIA PaCa-2 cells (CM-OE-NC) was used as a negative control. MIN6 cells were assessed for GSIS, intracellular insulin (mRNA and protein), and cell viability at 0-, 48-, and 72-hours post-treatment. To ensure the robustness and reproducibility of the observed phenotype and rule out off-target effects, we performed GSIS assays using CM from PANC-1 cells transfected with two distinct shRNAs per gene, each exhibiting different knockdown efficiencies. GSIS assays revealed that CM from NEK2-knockdown PANC-1 cells (CM-sh-NEK2#1/#2) significantly alleviated the suppression of insulin secretion in MIN6 cells induced by CM-sh-NC, with insulin secretion in MIN6 cells restored to control levels under both low- and high-glucose conditions (Fig. 4A). Similarly, insulin secretion in MIN6 cells treated with CM from PLK1-knockdown PANC-1 cells (CM-sh-PLK1#1/#2) was also restored to control levels, effectively reversing the impairment caused by CM-sh-NC (Fig. 4B). In gain-of-function studies, CM from MIA PaCa-2 cells overexpressing NEK2 (CM-OE-NEK2) or PLK1 (CM-OE-PLK1) significantly suppressed insulin secretion in MIN6 cells, whereas CM-OE-NC showed no such inhibitory effect (Fig. 4C).

We next examined insulin gene (*Ins1* and *Ins2*) expression and intracellular insulin content in MIN6 cells following CM treatment. Compared to control medium, MIN6 cells treated with CM-sh-NC exhibited significant reductions in *Ins1* and *Ins2* mRNA levels and insulin protein content (Figs. 4D-E, G-H). This suppression was effectively reversed by CM-sh-NEK2#1/#2, which restored both

Journal Pre-proof

mRNA and protein levels to those observed in the control medium group (Figs. 4D, G). Similarly, CM-sh-PLK1#1/#2 also restored insulin expression and content to control levels (Figs. 4E, H). Conversely, CM-OE-NEK2 or CM-OE-PLK1 significantly suppressed both insulin mRNA and protein levels in MIN6 cells relative to the CM-OE-NC group (Figs. 4F, I).

The viability of MIN6 cells was significantly suppressed following treatment with CM-sh-NC derived from PANC-1 cells (Figs. 4J, K). However, this inhibitory effect was markedly alleviated when MIN6 cells were treated with CM-sh-NEK2#1/#2 at 72 h post-treatment (Fig. 4J). A similar restoration of cell viability was observed with CM-sh-PLK1#1/#2 (Fig. 4K). In contrast, CM-OE-NEK2 or CM-OE-PLK1 further exacerbated the suppression of MIN6 cell viability compared to the CM-OE-NC group (Fig. 4L).

To further define the roles of NEK2 and PLK1 in PANC-1-derived CM-induced suppression of insulin content and impaired insulin secretion in MIN6 cells, PANC-1 cells were treated with increasing concentrations of the NEK2 inhibitor Nek2-IN-5 or the PLK1 inhibitor BI6727 for 72 h. The resulting CM was then collected and used to treat MIN6 cells, followed by GSIS and insulin content assays. Both Nek2-IN-5 and BI6727 significantly alleviated the inhibitory effects of PANC-1-derived CM on insulin secretion and insulin content in MIN6 cells in a dose-dependent manner (Figs. 4M-P).

These findings show that both NEK2 and PLK1 cause PaC cells-induced dysfunction of insulin secretion and inhibition of cell viability in MIN6 cells.

NEK2 and PLK1 cause PaC cell-induced dysfunction by inducing endoplasmic reticulum stress in MIN6 cells.

To elucidate the mechanism underlying PaC-induced β-cell impairment, we collected and analyzed

Journal Pre-proof

KEGG pathway analysis on RNA sequencing data from pancreatic islet cells of PaC patients with or without diabetes [18]. The results revealed significant enrichment of pathways related to protein processing in the ER, suggesting ER stress may contribute to islet β-cell dysfunction in PaCDM (Fig. S4A). We subsequently examined whether ER stress mediates the damaging effects of PaC cells on β cells using the ER stress inhibitor RH01386, which has been shown to ameliorate insulin secretion dysfunction and attenuate apoptosis by restoring ATP levels and suppressing caspase-3 activity in β cells [19]. CM-PANC-1 significantly upregulated the expression of ER stress markers (BiP, CHOP, and XBP1s) at both protein and mRNA levels in MIN6 cells (Figs. S4B-E). RH01386 treatment dose-dependently alleviated this ER stress induction, with 10 μM concentration effectively restoring marker expression to control levels (Figs. S4B-E). These results demonstrate that PANC-1 cells trigger ER stress in β cells, and identify ER stress as an important mechanism in PaC-induced β-cell impairment.

To determine whether NEK2 and PLK1 contribute to PANC-1-induced ER stress in β cells, we analyzed the expression of ER stress markers (*Bip*, *Chop*, and *Xbp1s*) in MIN6 cells treated with Ctrl, CM-sh-NC, CM-sh-PLK1#1, or CM-sh-NEK2#2. RT-qPCR analysis revealed that CM-sh-NC significantly upregulated all three ER stress markers compared to Ctrl, whereas both CM-sh-PLK1#1 and CM-sh-NEK2#2 restored their expression to control levels (Figs. 5A-C). Consistent results were obtained at the protein level by Western blot (Fig. 5D). In gain-of-function experiments, CM-OE-NEK2 significantly increased ER stress marker expression, and this effect was reversed by co-treatment with 10 μM RH01386 (Figs. 5E, F). Similarly, CM-OE-PLK1 also markedly induced ER stress, which was likewise alleviated by 10 μM RH01386 (Figs. 5G, H).

Given the dysregulation of CHOP, a key mediator of ER stress-induced apoptosis [7], we evaluated

MIN6 cell apoptosis by annexin V-FITC/PI staining. Compared with control cells, MIN6 cells treated with CM-sh-NC for 48 hours exhibited a significantly higher percentage of early and late apoptotic cells. In contrast, both CM-sh-PLK1#1 and CM-sh-NEK2#2 restored apoptosis rates to levels comparable to the control (Fig. 5I). Consistently, CM-OE-NEK2 and CM-OE-PLK1 significantly aggravated MIN6 cell apoptosis. This effect was markedly attenuated by co-treatment with 10 μM RH01386 (Figs. S4F, G), confirming the involvement of ER stress in NEK2/PLK1-mediated β-cell apoptosis.

As abnormal proinsulin accumulation represents another hallmark of ER stress in β cells [20], we examined its levels under different treatment conditions. MIN6 cells treated with CM-sh-NC showed significantly increased proinsulin protein levels, whereas both CM-sh-PLK1#1 and CM-sh-NEK2#2 restored proinsulin to control levels (Fig. 5J). Consistent with these findings, immunofluorescence analysis revealed enhanced proinsulin fluorescence intensity in MIN6 cells following CM-sh-NC treatment, while CM-sh-PLK1#1 and CM-sh-NEK2#2 maintained fluorescence intensity at control levels (Fig. 5K). In gain-of-function experiments, both CM-OE-NEK2 and CM-OE-PLK1 significantly elevated proinsulin protein levels and fluorescence intensity in MIN6 cells compared to CM-OE-NC. These effects were effectively reversed by 10 μM RH01386, which restored proinsulin accumulation to baseline levels (Figs. S4H-K).

To determine whether ER stress directly mediates the insulin secretion impairment induced by NEK2 and PLK1, we simultaneously assessed ER stress markers and insulin content in MIN6 cells under various treatments. This experimental approach was designed to capitalize on the strong correlation between intracellular insulin content and secretion capacity, while enabling co-detection of insulin and ER stress markers within the same samples. Consistent with our hypothesis, CM-

PANC-1 significantly upregulated ER stress markers while concurrently suppressing intracellular insulin content (Fig. S4B). Treatment with the ER stress inhibitor RH01386 produced a dose-dependent concomitant restoration: as ER stress marker expression decreased, insulin content progressively increased, with 10 μM RH01386 restoring insulin content to control levels (Fig. S4B). Importantly, this rescuing effect of RH01386 on both ER stress and insulin content was comparable to that achieved by NEK2 or PLK1 knockdown in PANC-1 cells (Figs. 4J, K and 5D). In complementary gain-of-function experiments, CM-OE-NEK2 and CM-OE-PLK1 simultaneously induced ER stress and suppressed insulin content in MIN6 cells (Figs. 5E-H). Critically, 10 μM RH01386 concurrently reversed both the elevated ER stress and the reduced insulin content, restoring them to levels observed in the control group (Figs. 5E-H).

These findings establish ER stress as an important mechanistic link between NEK2/PLK1 expression in PaC cells and the subsequent dysfunction in β cells, demonstrating that NEK2/PLK1 primarily induce ER stress, which in turn leads to reduced insulin content, impaired secretion function and overactivated apoptosis.

Silencing *Nek2* or *Plk1* in PaC cells alleviates PaC cells-induced glucose intolerance *in vivo*.

As *in vitro* modulation of NEK2 and PLK1 in PANC-1 and MIA PaCa-2 cells significantly altered pancreatic cancer cell-induced MIN6 cell impairment, with knockdown alleviating and overexpression exacerbating the impairment, and as this impairment was mediated by secreted factor(s) from these cells that triggered ER stress in MIN6 cells, we next asked whether NEK2 and PLK1 contribute to PaCDM-associated glucose intolerance *in vivo*. To this end, we established a mouse model by subcutaneously/orthotopically injecting Panc02 cells into C57BL/6 mice [5].

Journal Pre-proof

Twenty mice were randomly divided into four groups receiving: DMEM (control group), sh-NC-transfected Panc02 cells (sh-NC group), or Panc02 cells transfected with sh-Plk1 or sh-Nek2 (sh-Plk1 and sh-Nek2 groups).

Knockdown efficiency was confirmed by qRT-PCR in transfected Panc02 cells prior to injection (Figs. 6A, B). Then, as shown in Fig. 6C, fasting blood glucose (FBG) was monitored on days 7, 14, and 21 post-injection, and an intravenous glucose tolerance test (IGTT) was performed on day 25. Consequently, mice were sacrificed for fasting serum insulin test, and IHC of insulin and ER stress markers (BiP and CHOP) in pancreas area were performed.

All tumor-bearing groups developed subcutaneous/orthotopic tumors of comparable weight and size (Figs. 6D-E, L-M). By day 21, mice in the sh-NC group exhibited significantly higher FBG than those in the sh-Nek2 and sh-Plk1 groups (Figs. 6F, N). IGTT further revealed that both sh-Nek2 and sh-Plk1 groups showed significantly lower blood glucose levels at 30 and 45 minutes after glucose challenge compared to the sh-NC group (Figs. 6G-H, O). Additionally, fasting serum insulin levels, which were significantly reduced in the sh-NC group relative to the control group, were restored in both sh-Nek2 and sh-Plk1 groups (Figs. 6I, P). Consistent with the *in vitro* findings, IHC analysis of mouse pancreatic tissues showed that insulin content in pancreatic islets was significantly lower in the sh-NC group than in the control group, whereas the protein levels of the ER stress markers (BiP and CHOP) were markedly higher than those in the control group. Knockdown of Nek2 or Plk1 in Panc02 cells significantly alleviated these effects, restoring them to levels comparable to those in the control group (Figs. 6J-K, Q-R).

These results demonstrate that silencing *Nek2* or *Plk1* in PaC cells alleviates tumor-induced glucose intolerance and improves insulin levels *in vivo*.

Journal Pre-proof

Discussion

Early detection of PaC is critical for improving patient survival, with the growing population of new-onset DM representing a key target for screening efforts [21, 22]. However, distinguishing PaCDM from the more common T2DM remains challenging due to their overlapping clinical features [7]. A deeper understanding of the distinct pathogenesis of PaCDM is therefore essential to identify biomarkers that can facilitate early detection of PaC among individuals with new-onset DM [5, 7, 9, 10, 12, 23]. In this study, we applied the SSN method, an approach suitable for limited sequencing datasets [13], to construct a functional gene network for PaCDM. This led to the identification of 10 candidate genes, among which *NEK2* and *PLK1* were further validated as potential driver genes through stability analysis and GSIS assays. Clinically, both genes were significantly upregulated in PaC tissues, particularly in patients with PaCDM. Functionally, we demonstrated that NEK2 and PLK1 expression in PaC cells contributed to β-cell dysfunction, characterized by impaired insulin secretion, reduced insulin expression, and decreased cell viability. We further showed that these effects were mediated through ER stress activation: PANC-1 cells triggered ER stress in β cells, which was reversible upon RH01386 treatment. Knockdown of *NEK2* or *PLK1* in PANC-1 cells reduced ER stress markers, attenuated apoptosis, and normalized proinsulin accumulation, whereas their overexpression in MIA PaCa-2 cells exacerbated ER stress, effects that were similarly rescued by RH01386. Importantly, intracellular insulin content was inversely correlated with ER stress levels, and pharmacological inhibition of ER stress restored insulin content. *In vivo*, silencing *Nek2* or *Plk1* in Panc02 cells alleviated glucose intolerance and restored insulin levels in mice. Collectively, these findings establish *NEK2* and *PLK1* as driver genes of PaCDM and uncover ER stress as an important mechanism underlying their role in PaC-induced

β-cell dysfunction.

Elucidating the pathogenesis of PaCDM faces several methodological challenges. First, the scarcity of sequencing data from PaC tissues of patients with or without diabetes limits the applicability of conventional bioinformatics methods that require large sample sizes. Second, prior studies have often relied on peripheral blood samples [9, 23] or commercially available cell lines [5], which may not fully capture the tissue-specific gene expression patterns of pancreatic tumors. Third, traditional approaches typically focus on individual genes with substantial expression differences (e.g., >1.5-fold change) [5, 9], potentially overlooking key driver genes with modest expression changes but critical network roles. To overcome these limitations, we applied the SSN method to construct functional gene network using sequencing data from adjacent non-cancerous tissues (57 cases) and pancreatic cancer tissues (4 cases each from PaC and PaCDM groups). This approach identified 10 candidate genes involved in PaCDM pathogenesis, including *NEK2* and *PLK1*, which demonstrated robustness across varying statistical thresholds. Notably, neither *NEK2* nor *PLK1* showed significant differential expression ($0.66 < \text{fold change} < 1.5$) and would have been missed by conventional differential expression analysis. Experimental validation confirmed their functional roles, demonstrating strong consistency between computational predictions and biological evidence. The SSN method offers distinct advantages for studying complex diseases: it requires fewer samples than conventional approaches and can identify driver genes based on network topology rather than expression magnitude alone [13]. As SSN methodology continues to be refined and applied, it holds promise for uncovering pathogenic mechanisms in other complex diseases where traditional methods have shown limitations.

The choice of PaC cell lines is critical in PaCDM research, as their inherent molecular and functional

characteristics significantly influence experimental outcomes. Previous studies, including those identifying adrenomedullin [5] and microRNA-19a [24] as mediators of β-cell dysfunction, have consistently reported variable effects across different PaC cell lines. In our study, we similarly observed that CM from PANC-1 cells significantly impaired insulin secretion and downregulated insulin content in MIN6 cells, whereas BxPC-3 and MIA PaCa-2 cells showed minimal effects, consistent with clinical observations that only a subset of PaC patients develop diabetes [2-4]. This functional heterogeneity informed our experimental strategy: we performed knockdown experiments in PANC-1 cells, which inherently damage β cells, and overexpression studies in MIA PaCa-2 cells, which lack this intrinsic effect. This approach effectively avoided potential false-negative results that might occur from overexpressing genes in already highly damaging cells or knocking down genes in minimally effective ones. Our results demonstrated that NEK2/PLK1 knockdown in PANC-1 cells alleviated β-cell impairment, while their overexpression in MIA PaCa-2 cells induced dysfunction. These findings highlight the importance of matching cell line selection to experimental objectives in PaCDM research. We recommend using inherently damaging cell lines (e.g., PANC-1) for loss-of-function studies and non-damaging lines (e.g., MIA PaCa-2) for gain-of-function experiments. This strategic approach provides a framework for future investigations into PaCDM pathogenesis and other context-dependent disease mechanisms.

This study reveals a previously unrecognized role for *NEK2* and *PLK1* in PaCDM pathogenesis. While both serine/threonine kinases are established regulators of cell cycle progression and tumorigenesis [15, 25], their involvement in paracrine signaling between PaC cells and β cells represents a novel mechanistic insight. We observed significant overexpression of NEK2 and PLK1 in PaC tissues, particularly from PaCDM patients, suggesting their clinical relevance to new-onset

Journal Pre-proof

DM in PaC patients. Functionally, CM from PANC-1 cells induced comprehensive β-cell dysfunction, impairing insulin secretion, reducing intracellular insulin content, and decreasing cell viability. These effects were dependent on NEK2 and PLK1, as their knockdown alleviated the damage, while their overexpression in minimally damaging MIA PaCa-2 cells enhanced β-cell impairment. The physiological relevance was confirmed *in vivo*, where silencing either kinase in Panc02 tumors improved glucose tolerance and restored serum insulin levels. These findings extend the understanding of how PaC cells induce paraneoplastic β-cell dysfunction through secreted factors [3, 5, 7, 10, 24, 26, 27] by identifying NEK2 and PLK1 as important regulators of this process. More broadly, our work aligns with emerging evidence of kinase-mediated tumor-stroma interactions [28, 29] and reveals an underappreciated role for cell cycle regulators in modulating the secretory phenotype of cancer cells and their communication with the tissue microenvironment.

Our study demonstrates that ER stress in β cells serves as an important mediator of the β-cell dysfunction induced by NEK2 and PLK1 in PaC cells in PaCDM pathogenesis. While oxidative stress, inflammation, and Ras activation have been implicated in PaC-induced β-cell damage [7, 10, 24, 26, 27], the potential role of specific intracellular kinases from cancer cells, which act in a cell-autonomous manner, in initiating ER stress to mediate this paracrine effect was unknown. Pancreatic β-cells are particularly susceptible to ER stress due to their high biosynthetic demand for insulin production [30-32]. In this study, we demonstrated that CM from PANC-1 cells triggered severe ER stress in MIN6 cells, characterized by elevated ER stress markers, enhanced apoptosis, and abnormal proinsulin accumulation, phenotypes consistent with those induced by known ER stress inducers such as adrenomedullin [7] or tunicamycin [19]. Notably, either knockdown of *NEK2* or *PLK1* in PANC-1 cells or treatment with the ER stress inhibitor RH01386 significantly alleviated

these abnormalities. Conversely, overexpression of *NEK2* or *PLK1* in MIA PaCa-2 cells exacerbated ER stress in MIN6 cells, an effect similarly reversed by RH01386. Furthermore, ER stress is a well-documented cause of impaired insulin secretion in β cells, manifesting as reduced insulin mRNA levels, abnormal proinsulin accumulation, and decreased insulin content [20, 33]. Our findings demonstrated that CM from PaC cells overexpressing NEK2 or PLK1 significantly exacerbated ER stress in MIN6 cells, which was accompanied by a marked reduction in intracellular insulin content. Importantly, both knockdown of NEK2/PLK1 in PaC cells and treatment with the ER stress inhibitor RH01386 attenuated ER stress and concurrently restored insulin content, establishing a direct link between NEK2/PLK1-mediated ER stress and insulin deficiency in β cells. These findings align with clinical observations that diabetes often resolves after pancreaticoduodenectomy in PaC patients [3], as well as experimental evidence indicating that removal of ER stress inducers can restore β-cell function [20]. We conclude that NEK2 and PLK1 in PaC cells trigger ER stress in pancreatic β cells, leading to impaired proinsulin processing [20], proinsulin accumulation, reduced insulin content, and ultimately impaired insulin secretion. Chronic ER stress not only disrupts proinsulin processing and insulin secretion but also promotes apoptosis, thereby reducing β-cell viability (Fig. 7) [7]. Mechanistically, we propose that NEK2 and PLK1 may facilitate phosphorylation events that induce a pro-inflammatory tumor microenvironment [15, 25], which could further aggravate ER stress in β cells [20]. Additionally, ER stress disrupts ATP homeostasis, contributing to insulin secretory failure, a process potentially targeted by RH01386 via its unique ability to restore ATP-dependent insulin secretion [19, 34, 35]. The observed upregulation of CHOP and associated apoptosis further supports the role of ER stress in β-cell loss [36, 37]. In summary, our findings identify ER stress as an important pathway through which NEK2 and PLK1 in PaC

cells induce β-cell dysfunction in PaCDM, highlighting promising targets for future therapeutic strategies.

Several limitations should be considered in this study. First, while the SSN method enabled network construction with limited samples, it presents challenges in interpretability and may have constrained applicability to other disease contexts. Although both target groups originated from the same microarray dataset and were evaluated against a shared RNA-seq reference set following common preprocessing, residual cross-platform effects cannot be excluded. Further assessment in clinically well-characterized, single-platform cohorts would strengthen the generalizability of the SSN-based findings. Second, although we identified *NEK2* and *PLK1* as driver genes in PaCDM pathogenesis, their inability to be secreted and detected in peripheral circulation limits their utility as non-invasive biomarkers for early PaC screening. Third, secretome profiling of NEK2 and PLK1 revealed complex downstream secreted protein landscapes, with both shared and gene-specific molecules that may act through distinct signaling pathways. Consequently, the specific effector molecules in the CM responsible for inducing β-cell damage, as well as the detailed signaling pathways leading to ER stress (Fig. 7), remain to be elucidated, and how NEK2 and PLK1 mediate ER stress and β-cell dysfunction through their respective downstream factors cannot be clearly defined in this study. Further studies are planned to investigate these aspects in the context of each gene. Fourth, all functional assays were conducted using the mouse insulinoma MIN6 cell line due to the limited availability of human primary islets from healthy or paraneoplastic pancreatic tissues. Moreover, in the comparison of immunohistochemical findings between PaC and PaCDM tissues, although age, BMI, and available clinical and pathological variables were balanced between groups and included as covariates where appropriate, detailed information on diabetes duration and

glucose-lowering medication was not uniformly available for all patients because of the retrospective nature of the cohort. Future prospective studies with standardized collection of glycemic history and medication records will be needed to further refine the adjustment for diabetes-related confounders. Finally, a limitation of our *in vitro* paradigm is that an independent mock-CM prepared under identical conditions without producer cells, as well as separately glucose-matched medium, was not included. Although fresh serum-free RPMI-1640 and HPDE6-derived CM produced nearly identical responses in MIN6 cells, and the marked dysfunction induced by CM-PANC-1 makes nonspecific nutrient or metabolic effects unlikely to account for the major phenotype, residual confounding by nutrient depletion or metabolic by-products cannot be completely excluded. Future studies incorporating mock-CM and nutrient-matched controls will further strengthen causal inference.

Conclusion

In summary, this study identifies NEK2 and PLK1 as previously unrecognized driver genes linking pancreatic cancer to new-onset diabetes. NEK2 and PLK1 are upregulated in pancreatic cancer tissues, particularly in patients with new-onset diabetes, and act independently in pancreatic cancer cells to induce ER stress-mediated β-cell dysfunction through their secreted downstream effectors. These findings reveal a mechanism by which pancreatic cancer cells remotely impair β-cell function and, more importantly, suggest that the downstream secreted molecules of NEK2 and PLK1 may serve as candidate biomarkers for the early detection of pancreatic cancer in patients with new-onset diabetes, thereby addressing a critical unmet clinical need.

Journal Pre-proof

Methods

Constructing SSNs for different types of samples based on SSN method

The Agilent microarray dataset GSE61166 (GPL16956), containing 8 pancreatic cancer samples and 4 pancreatitis samples (12 samples in total), was obtained and subjected to filtering based on clinical information, resulting in the selection of 8 pancreatic cancer samples for analysis. The inclusion criteria were as follows: (1) histologically confirmed diagnosis of pancreatic cancer; and (2) availability of clear diabetes status and duration of diabetes. Patients with concomitant pancreatitis or those with a history of other malignancies were excluded. These 8 cancer samples were divided into two groups based on the presence or absence of PaCDM. The first group consisted of 4 samples of PaC group, while the second group comprised 4 samples of PaCDM group.

A set of 57 paraneoplastic samples of adjacent non-cancerous pancreatic tissue was considered as the reference samples for constructing the reference network. The RNA-seq data of the 57 paraneoplastic pancreatic tissues samples were obtained from the CPTAC-3 Project (46 samples) and the ORGANOID-PANCREATIC Project (11 samples) via the Genomic Data Commons (GDC) Data Portal (https://portal.gdc.cancer.gov/). Before SSN analysis, expression values from both the microarray target samples and the RNA-seq reference samples were subjected to the same $\log_2(x+1)$ transformation, where x denotes the input expression value. Gene identifiers were harmonized, and a common gene set was retained for subsequent network construction. The reference network was constructed by calculating the pairwise *PCC*s (Formula 1) [38] to represent the gene-gene interactions. In detail, for a group of reference samples (n samples), a reference network can be constructed by the correlations between genes based on expression data of reference

samples, i.e. computing the PCC_n (the *PCC* of an edge in the reference network with *n* samples) of each pair of genes as an edge in the network, which is similar to the method we conducted in previous study [13]. This reference network served as the baseline for subsequent differential network computations. To construct the SSNs, individual samples ($S^{'}_d$ and $S^{''}_d$) from the two groups of cancer samples (PaC and PaCDM) were extracted and added to the reference samples. This resulted in the formation of two types of perturbed samples. For each perturbed sample, the new pairwise *PCC*s, which were calculated as PCC_{n+1} with the addition of one individual sample ($S^{'}_d$ or $S^{''}_d$) to reference samples, were calculated to construct the corresponding perturbed network. Then, 8 independent perturbed networks were constructed, 4 for PaC group and 4 for PaCDM group.

$$r_{xy} = \frac{\sum_{i=1}^{n}(x_i - \bar{x})\,(y_i - \bar{y})}{\sqrt{\sum_{i=1}^{n}(x_i - \bar{x})^2}\sqrt{\sum_{i=1}^{n}(y_i - \bar{y})^2}} \quad (1)$$

Based on the SSN theory [13], the differential edges between the perturbed and reference networks were represented by $\Delta PCC_n = PCC_{n+1} - PCC_n$. A Z-test (Formula 2) was conducted to identify edges with significant differences after perturbing individual samples. Edges (p-value < 0.01 in the Z-test) were considered statistically significant, enabling the construction of individual-specific networks for each pancreatic cancer sample. Consequently, a total of 8 individual-specific networks (4 for PaC, 4 for PaCDM) were obtained for the two different types of samples.

$$Z = \frac{\Delta PCC_n}{(1 - PCC_n^2)/(n-1)} \quad (2)$$

Constructing a functional gene network and screening potential driver genes for PaCDM

The edges (gene-gene interactions) of the 8 individual-specific networks underwent an intersection alignment operation, and the shared edges in all 8 networks were preserved. This operation retained a total of 102,710 differential edges, and 8 SSNs (4 SSNs for PaC samples and 4 SSNs for PaCDM samples) were obtained. To identify significantly different edges between the two types of SSNs, a Paired-Samples T-test (Formula 3) with a *p*-value < 0.0001 was conducted.

$$t = \frac{\sum d}{\sqrt{\frac{n(\sum d^2) - (\sum d)^2}{n-1}}} \quad (3)$$

After the T-test, a total of 975 significantly different edges were retained and used to construct an important functional gene network, which was further analyzed to identify candidate genes as the potential functional driver genes. The selection of candidate genes was based on their degree value, representing the number of connections each gene has in the network. The top 10 genes with the highest degree value were considered as candidate genes. To further refine the candidate gene pool, we conducted candidate gene stability tests to reduce the randomness inherent in the SSN method results. Then candidate genes were further narrowed based on stability assessment in the network via adjusting the threshold of *p*-value of Paired-Samples T-test from 0.05 to 0.0001. The stability of candidate genes was confirmed by comparing the IQR of the variation range of degree values of candidate genes in the changing network. Finally, an IQR of less than 10 for candidate genes was used as a criterion for screening potential driver genes.

Python software was used to calculate the SSN and functional gene network. The scipy.stats module package was used to calculate the *PCC* of each gene pair. Cytoscape_v3.9.0 software was used to visualize the functional gene network. And process and code for the project was available at https://github.com/ZaakZoeng/SSN4PaCDM. The meaning of all symbols (e.g. rxy, n, d) in Equation 1-3 was explained in Additional file 3: The meaning of all symbols (e.g. rxy, n, d) in Equation 1-3.

Cells and cell culture

Human pancreatic cancer cell lines (BxPC-3 (Cat. TCHu 12), MIA PaCa-2 (Cat. SCSP-568), PANC-1 (Cat. TCHu 98)) and human embryonic kidney cells (HEK-293T (Cat. GNHu44)) were purchased from the Cell Bank of the Chinese Academy of Sciences (Shanghai, China). Mouse insulinoma MIN6 cells (Cat. BNCC338217) and human normal pancreatic duct epithelial cell line (HPDE6 (Cat. BNCC359453)) were purchased from Beijing Beina Chuanglian Biotechnology Research Institute. Mouse pancreatic cancer cell lines (Panc02 (Cat. CL-0736)) were purchased from Wuhan Pricella Biotechnology Co., Ltd. BxPC-3 cells were cultured in RPMI 1640 medium (Gibco). MIA PaCa-2, PANC-1, Panc02, HPDE6 and HEK-293T cells were cultured in high-glucose Dulbecco's Modified Eagle Medium (DMEM, Gibco). All media were supplemented with 10% fetal bovine serum (FBS, Gibco), 100 IU/mL penicillin and 100 μg/mL streptomycin (NCM, Suzhou, China). MIN6 cells were cultured in RPMI 1640 medium (Gibco), 10% FBS (ExCell Bio, Catalog no. FSP500), 100 μmol/L β-mercaptoethanol (Sigma, M3148). Cells were cultured at 37 °C, supplied with 5% CO_2.

Reagents

RH01386 (Cat. No. HY-124771, CAS No. 301177-36-6, molecular formula $C_{18}H_{15}F_3N_4O_3S$), a selective small-molecule ER stress inhibitor, was purchased from MedChemExpress (USA). It was

dissolved in dimethyl sulfoxide (DMSO) as a 10 mM stock solution and applied to MIN6 cells at concentrations ranging from 100 nM to 10 μM for 48 hours. RH01386 has been shown to ameliorate ER stress-induced β-cell dysfunction through two principal mechanisms: restoring GSIS by recovering ATP levels, and suppressing apoptosis via inhibition of caspase-3 activity [19]. Nek2-IN-5 (Cat. No. HY-120330, CAS No. 1507367-00-1, molecular formula $C_{15}H_{12}N_6O$), a potent and irreversible inhibitor of Nek2 (Never in mitosis gene A-related kinase 2), was purchased from MedChemExpress (USA). It was dissolved in DMSO to prepare a stock solution and applied to PANC-1 cells at the indicated concentrations for 72 hours. Nek2-IN-5 is a click chemistry reagent containing an alkyne group [39]. BI6727 (Volasertib) (Cat. No. HY-12137A, CAS No. 946161-17-7, molecular formula $C_{34}H_{53}Cl_3N_8O_3$), an orally active, highly potent and ATP-competitive Polo-like kinase 1 (PLK1) inhibitor with an IC_{50} of 0.87 nM, was purchased from MedChemExpress (USA). It was dissolved in DMSO to prepare a stock solution and applied to PANC-1 cells at the indicated concentrations for 72 hours. Volasertib is a dihydropteridinone derivative that induces mitotic arrest and apoptosis and shows marked antitumor activity in multiple cancer models [40].

Collection of conditioned media

HPDE6 and pancreatic cancer cells were expanded, washed twice with PBS, trypsinized, and counted. An equal number of viable cells (4×10^6 per 10 cm plate) was then re-seeded for each experimental group. After 12 h of attachment, the culture medium was replaced with 7 mL of serum-free RPMI 1640 medium per plate. The RPMI-1640 basal medium contained standard inorganic salts, amino acids, vitamins, and D-glucose at 2.0 g/L, and no serum or other supplements were added during CM collection. Following 48 h of incubation, the CM was collected and centrifuged at 3,000 rpm for 5 min at 4 °C to remove cellular debris/dead cells. The supernatant was aliquoted

and stored at -80 °C for use in subsequent experiments within two weeks [10].

Construction of a MIN6 cells treatment system

MIN6 cells were seeded in 24-well plates at 75,000 cells per well and maintained in triplicate for each treatment condition. After 12 h of attachment, the culture medium was replaced with 500 μL per well of either control medium or CM. The control medium consisted of fresh RPMI 1640 medium mixed with heat-inactivated FBS at a 10:1 ratio. CM was similarly supplemented with heat-inactivated FBS at a 10:1 ratio prior to use. Both media were refreshed every 24 hours. For experiments involving the ER stress inhibitor RH01386, the compound was dissolved in DMSO and diluted in CM to the desired concentration. To ensure consistent exposure, cells were co-treated with RH01386 and CM for 48 hours, with both media being replenished every 24 hours to maintain compound activity. An equivalent volume of DMSO was added to all other treatment groups to control for vehicle effects. After 48 hours of treatment, when MIN6 cells in the control group reached approximately 90% confluency, cells were harvested for subsequent protein and mRNA analysis [10, 41].

Glucose stimulated insulin secretion (GSIS) assay in MIN6 cells

GSIS assays were performed in MIN6 cells seeded in 24-well plates at a density of 75,000 cells per well, with two or three replicate wells per treatment condition. Cells were maintained in control or CM, refreshed every 24 hours as previously described. After 48 hours of treatment, cells were washed once with pre-warmed Krebs-Ringer bicarbonate (KRB) buffer (114 mM NaCl, 4.7 mM KCl, 1.2 mM KH_2PO_4, 1.16 mM $MgSO_4$, 25.5 mM $NaHCO_3$, 2.5 mM $CaCl_2$, 20 mM HEPES, 0.2% BSA, pH 7.4) [10, 20]. Subsequently, cells were incubated for 1 h at 37 °C in 250 μL/well of KRB buffer containing no glucose, followed by a 1 h incubation in KRB buffer supplemented with either

Journal Pre-proof

2.8 mM (low) or 16.8 mM (high) glucose. Supernatants were collected, centrifuged at 1,000 × g for 15 min at 4 °C, and 200 μL of the upper fraction was used for insulin quantification using a Mouse Insulin ELISA kit (CUSABIO, CSB-E05071m) according to the manufacturer's protocol [20]. Each experiment was independently repeated three times.

RNA extraction and real-time quantitative polymerase chain reaction (RT-qPCR)

Total RNA was extracted from harvested cells using RNA isolater Total RNA Extraction Reagent (Vazyme, Catalog no. R401-01) according to the manufacturer's instructions. The starting material consisted of 1-2 × 10^6 cells for human pancreatic cell lines (HPDE6, BxPC-3, MIA PaCa-2, PANC-1) and the mouse Panc02 cell line, and 6 × 10^5 cells for MIN6 cells. cDNA was synthesized from total RNA using the HiScript III 1st Strand cDNA Synthesis Kit (+gDNA wiper) (Vazyme, Catalog no. R312-01) with oligo(dT) primers. qRT-PCR was performed on a LightCycler® 480 II system (Roche, Switzerland) using SYBR qPCR Master Mix (Vazyme, Catalog no. Q711-02). The thermal cycling conditions were as follows: initial denaturation at 95 °C for 30 s, followed by 40 cycles of 95 °C for 5 s and 60 °C for 30 s. GAPDH and Actb were used as reference genes for human and mouse cells, respectively. Relative expression levels were calculated using the 2^(–ΔΔCt) method, with the control group set as 1 for normalization. All reactions were performed in triplicate. Primer sequences are provided in Table S1, and melting curves for each primer pair are shown in Additional file 4: The melting curves for each pair of primers.

Plasmid construction and cell transfection

For gene knockdown, two distinct shRNAs targeting each candidate gene were inserted into the CMV-copGFP-T2A-puro-H1-shRNA vector (sh-gene#1 and sh-gene#2; Bioegene, Shanghai,

Journal Pre-proof

China). A scrambled shRNA sequence (5'-TTCTCCGAACGTGTCACGT-3') was used as a negative control (sh-NC) [42]. For gene overexpression, the coding sequences of *NEK2* and *PLK1* were cloned into the pCDH-CMV vector (OE-NEK2-HA and OE-PLK1-Flag; Bioegene), with the empty vector serving as the overexpression-negative control (OE-NC). Lentiviruses were produced by co-transfecting the constructed plasmids with the packaging plasmid psPAX2 and the envelope plasmid pMD2.G into HEK-293T cells. Viral supernatants were harvested 48 hours post-transfection and filtered through 0.45 μm membranes (Millipore, USA). Target cells were infected with the lentiviral particles for 14 hours, followed by a 72-hour proliferation period. Stable cell lines were then selected using puromycin (10 μg/mL; Beyotime) for three days. The shRNA sequences used are provided in Table S2.

Western blotting

Proteins were extracted from human pancreatic cell lines (HPDE6, BxPC-3, MIA PaCa-2, PANC-1) using 1-2 × 10^6 cells per sample, and from mouse MIN6 cells using 3 × 10^5 cells. Cells were lysed in 1× Omni-Easy Protein Sample Loading Buffer (EpiZyme, Shanghai, China) for denaturation. Lysates were separated by SDS-PAGE on 7.5%, 10%, or 12.5% gels and transferred to PVDF membranes (Millipore, USA). After blocking, membranes were incubated with primary and secondary antibodies, and protein signals were detected using an ECL system (Tanon 5200; Shanghai Tanon Life Science Co., Ltd., China). To ensure equal loading, protein amounts were initially loaded at 10 μL per lane and adjusted as necessary based on the band intensity of the internal control until consistent signals were achieved. GAPDH and β-Actin served as internal controls for human and mouse cells, respectively. All antibodies are listed in Table S3. Each experiment was repeated three times independently, and representative raw blot images are provided in Additional

Journal Pre-proof

file 2: Raw image files of Western blotting.

Cell viability assay

MIN6 cells were seeded in 96-well plates at a density of 1,750 cells per well and allowed to adhere for 12 h. The culture medium was then replaced with 100 μL of control or CM, which was refreshed every 24 h. Cell viability was assessed at 0, 48, and 72 h after treatment initiation using a Cell Counting Kit-8 (CCK-8; Beyotime, Shanghai) according to the manufacturer's instructions. All experiments were performed in three independent replicates.

Immunofluorescence staining (IF)

MIN6 cells were seeded on glass microscope cover slips (NEST) in 24-well plates at 75,000 cells per well and treated with control or CM for 48 h. After treatment, cells were washed twice with pre-cooled PBS and fixed overnight at 4 °C with 4% paraformaldehyde. Following fixation, cells were permeabilized with 0.1% Triton X-100 in PBS for 30 min at room temperature and blocked with 5% BSA in 1×T-PBS for 30 min at room temperature. Then, cells were incubated overnight at 4 °C with a mouse anti-Proinsulin antibody (Novus Biologicals, 253627; 25 μg/mL) diluted in blocking solution. After washing, a Cy3-conjugated goat anti-mouse secondary antibody (Abcam, ab97035; 1:400 dilution in PBS) was applied and incubated for 1 h at room temperature in the dark. Nuclei were counterstained with DAPI (Beyotime, C1006; 1:5000 dilution in PBS) for 5-10 min at room temperature in the dark. Staining intensity was monitored under a fluorescence microscope, and DAPI was removed when optimal nuclear staining was achieved. Anti-fade mounting medium was applied, and coverslips were carefully inverted onto glass slides for sealing. Images were acquired using a confocal laser scanning microscope (Leica SP8 confocal microscope) (Excitation/Emission wavelengths: DAPI - 405 nm/415-564 nm; Cy3 - 561 nm/566-716 nm) and analyzed with dedicated

software (Leica Application Suite X). The proinsulin signal is displayed in green pseudocolor; DAPI is shown in blue. The emission spectrum of green channel (anti-Proinsulin antibody) is presented in Additional file 5: The emission spectrum of green channel.

Annexin V-FITC/PI staining

MIN6 cells were seeded in 24-well plates at 75,000 cells per well and treated with control or CM for 48 h as previously described. After treatment, cells were harvested by trypsinization, washed, and resuspended in 1×binding buffer from the Annexin V-FITC/PI Apoptosis Detection Kit (Yeasen, China). Staining was performed according to the manufacturer's instructions. Flow cytometry was conducted on a flow cytometer CytoFlex LX (BECKMAN, USA). Fluorescence spillover compensation was performed using single-color controls for FITC and PI. Compensation matrices were created and applied to all experimental data using FlowJo 10.8.1 software to eliminate spectral overlap between channels. A minimum of 10,000 events were acquired per sample. FITC was excited at 488 nm and detected with a 525/40 nm band-pass filter, while PI used 561 nm excitation and a 610/20 nm band-pass detection filter. Data analysis was performed using FlowJo 10.8.1 software. All experiments were repeated three times independently.

Tissue sample collection

Paraffin-embedded pancreatic tumor tissue samples were obtained from 163 pancreatic cancer patients who underwent pancreatectomy at the Second Affiliated Hospital of Zhejiang University between January 2013 and December 2017. Among these patients, 108 were without diabetes (PaC group) and 55 had new-onset diabetes (PaCDM group). The diagnostic criteria for DM were in accordance with the American Diabetes Association [43]. Additionally, 15 patients had adjacent paraneoplastic pancreatic tissue samples collected in addition to their pancreatic tumor tissue

Journal Pre-proof

samples. All tissue samples were utilized for immunohistochemical staining. Written informed consent was obtained from all participants for the use of clinical samples in medical research. The study protocol was approved by the Ethics Committee of the Second Affiliated Hospital of Zhejiang University (Approval No. I2019001590). Clinical trial number: not applicable.

Immunohistochemical (IHC) staining

IHC staining was performed using the standard streptavidin-biotin-peroxidase complex method. Paraffin-embedded tissue sections were deparaffinized, rehydrated, and subjected to antigen retrieval by heating in 10 mM citrate buffer (pH 6.0) for 15 min. Sections were then incubated overnight at 4 °C with primary antibodies against PLK1 (1:50 dilution, Cell Signaling, 4513S), NEK2 (1:500 dilution, Abcam, ab227958), or Insulin (1:32,000 dilution, Abcam, ab181547). Detection was carried out using the EnVision Plus System-HRP (DAB; DAKO) according to the manufacturer's instructions, followed by counterstaining with Mayer's hematoxylin. Stained slides were scanned and viewed using CaseViewer 2.4 software.

IHC scoring was based on the percentage of positive cells (0 = 0%; 1 = 1-20%; 2 = 21-50%; 3 = 51-80%; 4 = 81-100%) and staining intensity (0 = negative; 1 = weak; 2 = moderate; 3 = strong). The final score for each sample was calculated by multiplying the percentage and intensity scores, and results were expressed as the mean of the total scores rounded to the nearest integer.

Experimental animals and in vivo protocol

Four- to six-week-old female C57BL/6 mice (n=20) were randomly assigned to four groups: control, sh-NC, sh-Plk1, and sh-Nek2. Control mice received a subcutaneous/orthotopic injection of 100 μL/50 μL DMEM, while the other three groups were injected subcutaneously/ orthotopically with 100 μL/50 μL of Panc02 cells (4×10^7 cells/mL/2.5 x 10^6 cells/mL) pre-treated with sh-NC, sh-Plk1,

or sh-Nek2, respectively. FBG was measured weekly starting one day after injection. Mice were fasted from 9:00 AM, and blood glucose was assessed via tail vein sampling at 5:00 PM using a glucometer (yuwell, China). An IGTT was conducted on day 25 post-injection by administering 5% glucose solution (1.5 mg glucose/g body weight) into the tail vein. Blood glucose levels were measured at 30, 45, 60, 75, and 90 minutes after glucose administration. On day 30, mice were fasted for 8 h and sacrificed. Blood was collected via orbital venous puncture, kept at room temperature for 2 h, and centrifuged at 3,000 rpm for 15 min to obtain serum. Serum insulin levels were determined using a mouse insulin ELISA kit (CUSABIO, CSB-E05071m). And pancreas of mice were obtained for further IHC staining.

All animal procedures were approved by the Ethics Committee of the Second Affiliated Hospital of Zhejiang University School of Medicine and conducted in accordance with institutional guidelines.

Co-immunoprecipitation (Co-IP)

MIA PaCa-2 cells were co-transfected with plasmids encoding NEK2-HA and PLK1-Flag using Lipofectamine 3000 (Invitrogen) according to the manufacturer's instructions. Forty-eight hours post-transfection, cells were washed twice with ice-cold PBS and lysed in IP lysis buffer (25 mM Tris-HCl pH 7.4, 150 mM NaCl, 1 mM EDTA, 1% NP-40, 5% glycerol) supplemented with protease and phosphatase inhibitor cocktails. Lysates were centrifuged at 16,000 × g for 15 min at 4°C, and protein concentrations were determined by BCA assay. Equal amounts of lysate (500-1000 μg) were pre-cleared with control agarose beads for 1 h at 4°C, then incubated overnight at 4°C with anti-HA agarose beads (Sigma-Aldrich) or anti-Flag M2 affinity gel (Sigma-Aldrich) for reciprocal Co-IP. After incubation, beads were washed five times with IP wash buffer (50 mM Tris-HCl pH 8.0, 300 mM NaCl, 0.5% Triton X-100). Bound proteins were eluted by boiling in 1x SDS sample buffer for

10 min, separated by SDS-PAGE, and transferred to PVDF membranes.

Data-independent acquisition mass spectrometry (DIA-MS)

CM was collected from PANC-1 cells transfected with sh-NC, sh-NEK2#2, or sh-PLK1#1 (three biological replicates per group) cultured in serum-free RPMI 1640 medium. The collected CM was centrifuged at 1,200 x g for 20 min at 4°C to remove cell debris, and the cleared supernatants were stored at -80°C until further processing. Secreted proteins were concentrated using Amicon Ultra centrifugal filters (3 kDa MWCO; Millipore) and subjected to trypsin digestion. The resulting peptides were desalted and analyzed by liquid chromatography-tandem mass spectrometry on an Orbitrap mass spectrometer operating in DIA mode. Peptides were separated on a nanoscale C18 reverse-phase column using a linear gradient of buffer B (80% acetonitrile and 0.1% formic acid) at a constant flow rate of 300 nL/min. The mass spectrometer was operated in DIA mode with a full MS scan (m/z 350-1,650) followed by MS/MS DIA scan events using stepped HCD collision energies of 25.5, 27, and 30% and an Orbitrap resolution of 30,000. DIA data were processed using DIA-NN software (version 1.8) in library-free mode against the human UniProt database for protein identification and quantification. Differentially secreted proteins were identified based on significance thresholds.

Statistical analysis

Statistical analyses were conducted using SPSS 26.0 (IBM, USA) and GraphPad Prism 8.0. Data from three independent experiments are presented as mean ± standard deviation (SD). Group differences were evaluated by Student's t-test, except for CCK-8 assay data which were analyzed using one-way ANOVA. $p < 0.05$ was considered to be statistically significant.

Journal Pre-proof

Declarations

Ethics approval and consent to participate

After deliberation by the Ethics Committee of the Second Affiliated Hospital of Zhejiang University, the collection and application of human samples was performed in accordance with the principles of the Helsinki Declaration. The study has been granted ethics committee of the Second Affiliated Hospital of Zhejiang University on 26 December 2019, with the ethical number I2019001590. All animal experiments in this study were conducted following the guidelines of the Basel Declaration and approved by the Second Affiliated Hospital of Zhejiang University–Animal Ethics Committee (Approval no. AIRB-2022-0704; Date: 24 December 2022).

Consent for publication

Not applicable

Availability of data and materials

The Agilent microarray data for 8 pancreatic cancer samples, comprising four samples from patients with diabetes and four from patients without diabetes, were obtained from GSE61166 in the GEO database. The RNA-seq expression data for the 57 adjacent non-cancerous pancreatic tissue samples were obtained from the CPTAC-3 Project (46 samples) and ORGANOID-PANCREATIC Project (11 samples) through the GDC Data Portal (https://portal.gdc.cancer.gov/). The associated metadata are available at the following link: https://github.com/ZaakZoeng/SSN4PaCDM/blob/main/data/raw_data_57_reference_samples_metadata.json. The KEGG analysis of differentially expressed genes in pancreatic islet cells from PaC patients with or without diabetes was acquired following article. Wigger L, Barovic M, Brunner AD, Marzetta F, Schöniger E, Mehl F, et al. Multi-omics profiling of living human pancreatic islet donors

reveals heterogeneous beta cell trajectories towards type 2 diabetes. Nature metabolism. 2021;3(7):1017-31. https://doi.org/10.1038/s42255-021-00420-9.

Competing interests

The authors declare that they have no competing interests.

Funding

This work was supported by the National Natural Science Foundation of China under grants No. 82272954, 82573736 (Yulian Wu), T2341024 (Xiaoping Liu), 82572303 (Xiawei Li); the National Key Research and Development Program of China (2022YFA1004800); Zhejiang Provincial Natural Science Foundation of China under Grant No. LZ22C060001 and the research funds of Hangzhou Institute for advanced study, UCAS (No. 2022ZZ01013, No. 2024HIAS-Y016).

CRediT authorship contribution statement

JYL, ZYF, XWL, XPL and YLW provided the conceptual framework for the study. JYL was responsible for experiments designing, data grouping, basic experiment implementation, data collation and article writing. ZZ and XPL were responsible for applying mathematical methods for gene network construction and statistical analysis. XWL and YLW were responsible for the adjustment of experimental protocols and the polishing of article. HCY, YHT, YJS, JLG and ZYF contributed to the implement of glucose stimulated insulin secretion test and subcutaneous injection of Panc02 cells in mice. MHSG and KYP contributed to the measurement of fasting blood glucose in mice. NW assisted in establishing stable-transfected PaC cells and performing extraction of total RNA from MIN6 cells and reverse transcription to generate cDNA. CML and KLC performed qRT-PCR experiments to validate primer specificity by analyzing melting curves for target genes and evaluate mRNA expression levels of *Xbp1s* across samples, respectively. XWL, YLW and XPL

Journal Pre-proof

supervised the project with input from JYL, ZZ, ZYF.

Acknowledgements

We extend our sincere gratitude to Dr. Xiaofen Jin of the Central Laboratory, Women's Hospital, School of Medicine, Zhejiang University, for her expert technical guidance in confocal imaging acquisition through Leica SP8 confocal microscope and record of emission spectra through Leica Application Suite X software, which proved essential for ensuring spectral fidelity in our experimental system.

Clinical trial number

Not applicable.

Declaration of Generative AI and AI-assisted technologies

During the preparation of this work, the authors used DeepSeek solely for grammar and language correction. After using this tool, the authors reviewed and edited the content as needed and take full responsibility for the final content of the publication.

Reference

[1] S.T. Chari, C.L. Leibson, K.G. Rabe, J. Ransom, M. de Andrade, G.M. Petersen, Probability of pancreatic cancer following diabetes: A population-based study, Gastroenterology 129(2) (2005) 504-11. https://doi.org/10.1016/j.gastro.2005.05.007

[2] S.T. Chari, C.L. Leibson, K.G. Rabe, L.J. Timmons, J. Ransom, M. de Andrade, et al., Pancreatic cancer-associated diabetes mellitus: Prevalence and temporal association with diagnosis of cancer, Gastroenterology 134(1) (2008) 95-101. https://doi.org/10.1053/j.gastro.2007.10.040

[3] R. Pannala, J.B. Leirness, W.R. Bamlet, A. Basu, G.M. Petersen, S.T. Chari, Prevalence and clinical profile of pancreatic cancer-associated diabetes mellitus, Gastroenterology 134(4) (2008)

Journal Pre-proof

981-7. https://doi.org/10.1053/j.gastro.2008.01.039

[4] G. Aggarwal, P. Kamada, S.T. Chari, Prevalence of diabetes mellitus in pancreatic cancer compared to common cancers, Pancreas 42(2) (2013) 198-201. https://doi.org/10.1097/MPA.0b013e3182592c96

[5] G. Aggarwal, V. Ramachandran, N. Javeed, T. Arumugam, S. Dutta, G.G. Klee, et al., Adrenomedullin is up-regulated in patients with pancreatic cancer and causes insulin resistance in β cells and mice, Gastroenterology 143(6) (2012) 1510-1517.e1. https://doi.org/10.1053/j.gastro.2012.08.044

[6] M. Pelaez-Luna, N. Takahashi, J.G. Fletcher, S.T. Chari, Resectability of presymptomatic pancreatic cancer and its relationship to onset of diabetes: A retrospective review of ct scans and fasting glucose values prior to diagnosis, The American journal of gastroenterology 102(10) (2007) 2157-63. https://doi.org/10.1111/j.1572-0241.2007.01480.x

[7] N. Javeed, G. Sagar, S.K. Dutta, T.C. Smyrk, J.S. Lau, S. Bhattacharya, et al., Pancreatic cancer-derived exosomes cause paraneoplastic β-cell dysfunction, Clinical cancer research : an official journal of the American Association for Cancer Research 21(7) (2015) 1722-33. https://doi.org/10.1158/1078-0432.ccr-14-2022

[8] J. Bao, D. Liu, J. Sun, X. Su, H. Cheng, L. Qi, et al., Pancreatic cancer-associated diabetes mellitus is characterized by reduced β-cell secretory capacity, rather than insulin resistance, Diabetes research and clinical practice 185 (2022) 109223. https://doi.org/10.1016/j.diabres.2022.109223

[9] H. Huang, X. Dong, M.X. Kang, B. Xu, Y. Chen, B. Zhang, et al., Novel blood biomarkers of pancreatic cancer-associated diabetes mellitus identified by peripheral blood-based gene expression

profiles, The American journal of gastroenterology 105(7) (2010) 1661-9. https://doi.org/10.1038/ajg.2010.32

[10] M. Kang, W. Qin, M. Buya, X. Dong, W. Zheng, W. Lu, et al., Vnn1, a potential biomarker for pancreatic cancer-associated new-onset diabetes, aggravates paraneoplastic islet dysfunction by increasing oxidative stress, Cancer letters 373(2) (2016) 241-50. https://doi.org/10.1016/j.canlet.2015.12.031

[11] J. Su, W. Pang, A. Zhang, L. Li, W. Yao, X. Dai, Exosomal mir-19a decreases insulin production by targeting neurod1 in pancreatic cancer associated diabetes, Molecular biology reports 49(3) (2022) 1711-1720. https://doi.org/10.1007/s11033-021-06980-z

[12] L. Tan, X. Ye, Y. Zhou, M. Yu, Z. Fu, R. Chen, et al., Macrophage migration inhibitory factor is overexpressed in pancreatic cancer tissues and impairs insulin secretion function of β-cell, Journal of translational medicine 12 (2014) 92. https://doi.org/10.1186/1479-5876-12-92

[13] X. Liu, Y. Wang, H. Ji, K. Aihara, L. Chen, Personalized characterization of diseases using sample-specific networks, Nucleic acids research 44(22) (2016) e164. https://doi.org/10.1093/nar/gkw772

[14] J. Xia, H. Zhao, J.L. Edmondson, B. Koss, F. Zhan, Role of nek2 in tumorigenesis and tumor progression, Trends in molecular medicine 31(1) (2025) 79-93. https://doi.org/10.1016/j.molmed.2024.07.013

[15] S. Iliaki, R. Beyaert, I.S. Afonina, Polo-like kinase 1 (plk1) signaling in cancer and beyond, Biochemical pharmacology 193 (2021) 114747. https://doi.org/10.1016/j.bcp.2021.114747

[16] Y. Cheng, H. Zhu, J. Ren, H.Y. Wu, J.E. Yu, L.Y. Jin, et al., Follicle-stimulating hormone orchestrates glucose-stimulated insulin secretion of pancreatic islets, Nature communications 14(1)

(2023) 6991. https://doi.org/10.1038/s41467-023-42801-6

[17] L. Cao, C. Huang, D. Cui Zhou, Y. Hu, T.M. Lih, S.R. Savage, et al., Proteogenomic characterization of pancreatic ductal adenocarcinoma, Cell 184(19) (2021) 5031-5052.e26. https://doi.org/10.1016/j.cell.2021.08.023

[18] L. Wigger, M. Barovic, A.D. Brunner, F. Marzetta, E. Schöniger, F. Mehl, et al., Multi-omics profiling of living human pancreatic islet donors reveals heterogeneous beta cell trajectories towards type 2 diabetes, Nature metabolism 3(7) (2021) 1017-1031. https://doi.org/10.1038/s42255-021-00420-9

[19] K. Tran, Y. Li, H. Duan, D. Arora, H.Y. Lim, W. Wang, Identification of small molecules that protect pancreatic β cells against endoplasmic reticulum stress-induced cell death, ACS chemical biology 9(12) (2014) 2796-806. https://doi.org/10.1021/cb500740d

[20] C.W. Chen, B.J. Guan, M.R. Alzahrani, Z. Gao, L. Gao, S. Bracey, et al., Adaptation to chronic er stress enforces pancreatic β-cell plasticity, Nature communications 13(1) (2022) 4621. https://doi.org/10.1038/s41467-022-32425-7

[21] A.D. Singhi, E.J. Koay, S.T. Chari, A. Maitra, Early detection of pancreatic cancer: Opportunities and challenges, Gastroenterology 156(7) (2019) 2024-2040. https://doi.org/10.1053/j.gastro.2019.01.259

[22] L. Wang, F.I. Scott, B. Boursi, K.A. Reiss, S. Williams, H. Glick, et al., Cost-effectiveness of a risk-tailored pancreatic cancer early detection strategy among patients with new-onset diabetes, Clinical gastroenterology and hepatology : the official clinical practice journal of the American Gastroenterological Association 20(9) (2022) 1997-2004.e7. https://doi.org/10.1016/j.cgh.2021.10.037

Journal Pre-proof

[23] X. Dai, W. Pang, Y. Zhou, W. Yao, L. Xia, C. Wang, et al., Altered profile of serum micrornas in pancreatic cancer-associated new-onset diabetes mellitus, Journal of diabetes 8(3) (2016) 422-33. https://doi.org/10.1111/1753-0407.12313

[24] W. Pang, W. Yao, X. Dai, A. Zhang, L. Hou, L. Wang, et al., Pancreatic cancer-derived exosomal microrna-19a induces β-cell dysfunction by targeting adcy1 and epac2, International journal of biological sciences 17(13) (2021) 3622-3633. https://doi.org/10.7150/ijbs.56271

[25] X. Huang, G. Zhang, T. Tang, X. Gao, T. Liang, One shoot, three birds: Targeting nek2 orchestrates chemoradiotherapy, targeted therapy, and immunotherapy in cancer treatment, Biochimica et biophysica acta. Reviews on cancer 1877(2) (2022) 188696. https://doi.org/10.1016/j.bbcan.2022.188696

[26] J. Gong, X. Li, Z. Feng, J. Lou, K. Pu, Y. Sun, et al., Sorcin can trigger pancreatic cancer-associated new-onset diabetes through the secretion of inflammatory cytokines such as serpin e1 and ccl5, Experimental & molecular medicine 56(11) (2024) 2535-2547. https://doi.org/10.1038/s12276-024-01346-4

[27] Z. Feng, J. Lou, C. Lin, H. Yu, Y. Tu, J. Gong, et al., Unraveling the role of mdk-sdc4 interaction in pancreatic cancer-associated new-onset diabetes by single-cell transcriptomic analysis, Advanced science (Weinheim, Baden-Wurttemberg, Germany) 12(39) (2025) e09987. https://doi.org/10.1002/advs.202409987

[28] Y. Cheng, F. Sun, D.V. Alapat, V. Wanchai, D. Mery, W. Guo, et al., High nek2 expression in myeloid progenitors suppresses t cell immunity in multiple myeloma, Cell reports. Medicine 4(10) (2023) 101214. https://doi.org/10.1016/j.xcrm.2023.101214

[29] Y. Zhou, L. Xu, Z. Wang, H. Liu, X. Zhang, C. Shu, et al., Sequentially targeting and intervening

Journal Pre-proof

mutual polo-like kinase 1 on cafs and tumor cells by dual targeting nano-platform for cholangiocarcinoma treatment, Theranostics 12(8) (2022) 3911-3927. https://doi.org/10.7150/thno.70557

[30] D. Scheuner, R.J. Kaufman, The unfolded protein response: A pathway that links insulin demand with beta-cell failure and diabetes, Endocrine reviews 29(3) (2008) 317-33. https://doi.org/10.1210/er.2007-0039

[31] D.L. Eizirik, M. Cnop, Er stress in pancreatic beta cells: The thin red line between adaptation and failure, Science signaling 3(110) (2010) pe7. https://doi.org/10.1126/scisignal.3110pe7

[32] S.G. Fonseca, J. Gromada, F. Urano, Endoplasmic reticulum stress and pancreatic β-cell death, Trends in endocrinology and metabolism: TEM 22(7) (2011) 266-74. https://doi.org/10.1016/j.tem.2011.02.008

[33] M. Blanc, L. Habbouche, P. Xiao, C. Lebeaupin, M. Janona, N. Vaillant, et al., Bax inhibitor-1 preserves pancreatic β-cell proteostasis by limiting proinsulin misfolding and programmed cell death, Cell death & disease 15(5) (2024) 334. https://doi.org/10.1038/s41419-024-06701-x

[34] M. Rocha, N. Diaz-Morales, S. Rovira-Llopis, I. Escribano-Lopez, C. Bañuls, A. Hernandez-Mijares, et al., Mitochondrial dysfunction and endoplasmic reticulum stress in diabetes, Current pharmaceutical design 22(18) (2016) 2640-9. https://doi.org/10.2174/1381612822666160209152033

[35] J.H. Lee, J. Lee, Endoplasmic reticulum (er) stress and its role in pancreatic β-cell dysfunction and senescence in type 2 diabetes, International journal of molecular sciences 23(9) (2022) 4843. https://doi.org/10.3390/ijms23094843

[36] S. Oyadomari, A. Koizumi, K. Takeda, T. Gotoh, S. Akira, E. Araki, et al., Targeted disruption

Journal Pre-proof

of the chop gene delays endoplasmic reticulum stress-mediated diabetes, The Journal of clinical investigation 109(4) (2002) 525-32. https://doi.org/10.1172/jci14550

[37] B. Song, D. Scheuner, D. Ron, S. Pennathur, R.J. Kaufman, Chop deletion reduces oxidative stress, improves beta cell function, and promotes cell survival in multiple mouse models of diabetes, The Journal of clinical investigation 118(10) (2008) 3378-89. https://doi.org/10.1172/jci34587

[38] K. Pearson, F. Galton, Vii. Note on regression and inheritance in the case of two parents, Proceedings of the Royal Society of London 58(347-352) (1895) 240-242. https://doi.org/10.1098/rspl.1895.0041

[39] H. Lebraud, C.R. Coxon, V.S. Archard, C.M. Bawn, B. Carbain, C.J. Matheson, et al., Model system for irreversible inhibition of nek2: Thiol addition to ethynylpurines and related substituted heterocycles, Organic & biomolecular chemistry 12(1) (2014) 141-8. https://doi.org/10.1039/c3ob41806e

[40] F.F. Xie, S.S. Pan, R.Y. Ou, Z.Z. Zheng, X.X. Huang, M.T. Jian, et al., Volasertib suppresses tumor growth and potentiates the activity of cisplatin in cervical cancer, American journal of cancer research 5(12) (2015) 3548-59. https://doi.org/ajcr.us/files/ajcr0018183

[41] M. Xue, Y. Zhu, Y. Jiang, L. Han, M. Shi, R. Su, et al., Schwann cells regulate tumor cells and cancer-associated fibroblasts in the pancreatic ductal adenocarcinoma microenvironment, Nature communications 14(1) (2023) 4600. https://doi.org/10.1038/s41467-023-40314-w

[42] S.P. Zielske, M. Stevenson, Importin 7 may be dispensable for human immunodeficiency virus type 1 and simian immunodeficiency virus infection of primary macrophages, Journal of virology 79(17) (2005) 11541-6. https://doi.org/10.1128/jvi.79.17.11541-11546.2005

[43] American Diabetes Association Professional Practice Committee for Diabetes, 2. Classification

Journal Pre-proof

and diagnosis of diabetes: Standards of medical care in diabetes-2018, Diabetes care 41(Suppl 1) (2018) S13-s27. https://doi.org/10.2337/dc18-S002

Table

Table 1 Clinicopathological characteristics of PaC and PaCDM group

Variables		PaC (n=108)	PaCDM (n=55)	*p*
Age (years)	Mean ± SD	62.7 ± 10.5	62.5 ± 10.9	0.93
Gender	Male (%)	68 (63.0)	34 (61.8)	0.885
	Female (%)	40 (37.0)	21 (38.2)	
BMI (kg/m^2)	Median (IQR)	22.02 (19.94-23.6)	22.89 (20.7-25.04)	0.061
Tumor diameter (cm)	Median (IQR)	3 (2.4-4)	3 (2.5-4)	0.231
TNM stage (AJCC 8th)	I(%)	56 (51.9)	19 (34.5)	0.064
	II(%)	41 (38.0)	25 (45.5)	
	III(%)	11 (10.2)	11 (20.0)	
	IV(%)	0 (0)	0 (0)	
T stage	1(%)	22 (20.4)	9 (16.4)	0.665
	2(%)	67 (62.0)	32 (58.2)	
	3(%)	18 (16.7)	13 (23.6)	
	4(%)	1 (0.9)	1 (1.8)	
N stage	0(%)	64 (59.3)	25 (45.5)	0.098
	1(%)	34 (31.5)	19 (34.5)	
	2(%)	10 (9.3)	11 (20.0)	
M stage	0(%)	108 (100)	55 (100)	NA
	1(%)	0 (0)	0 (0)	
Vascular invasion	No (%)	58 (53.7)	27 (49.1)	0.578
	Yes (%)	50 (46.3)	28 (50.9)	
Perineural invasion	No (%)	25 (23.1)	11 (20.0)	0.646
	Yes (%)	83 (76.9)	44 (80.0)	
Adipose tissue invasion	No (%)	61 (56.5)	33 (60.0)	0.668
	Yes (%)	47 (43.5)	22 (40.0)	
Differentiation	Well (%)	27 (25.0)	9 (16.4)	0.263
	Moderate (%)	71 (65.7)	44 (80.0)	
	Poor (%)	9 (8.3)	2 (3.6)	
	Undifferentiated (%)	1 (1.0)	0 (0)	

Data are presented as mean ± SD for approximately normally distributed variables, median (IQR) for skewed variables, and n (%) for categorical variables. Age was compared using the independent-samples T-test; BMI and tumor diameter were compared using the Mann-Whitney U test; categorical variables were compared using the chi-square test or Fisher's exact test where appropriate. M stage

was not tested because all patients were M0. PaC, pancreatic cancer without diabetes; PaCDM, pancreatic cancer-associated diabetes; BMI, body mass index; IQR, interquartile range; NA, not applicable.

Figure legends

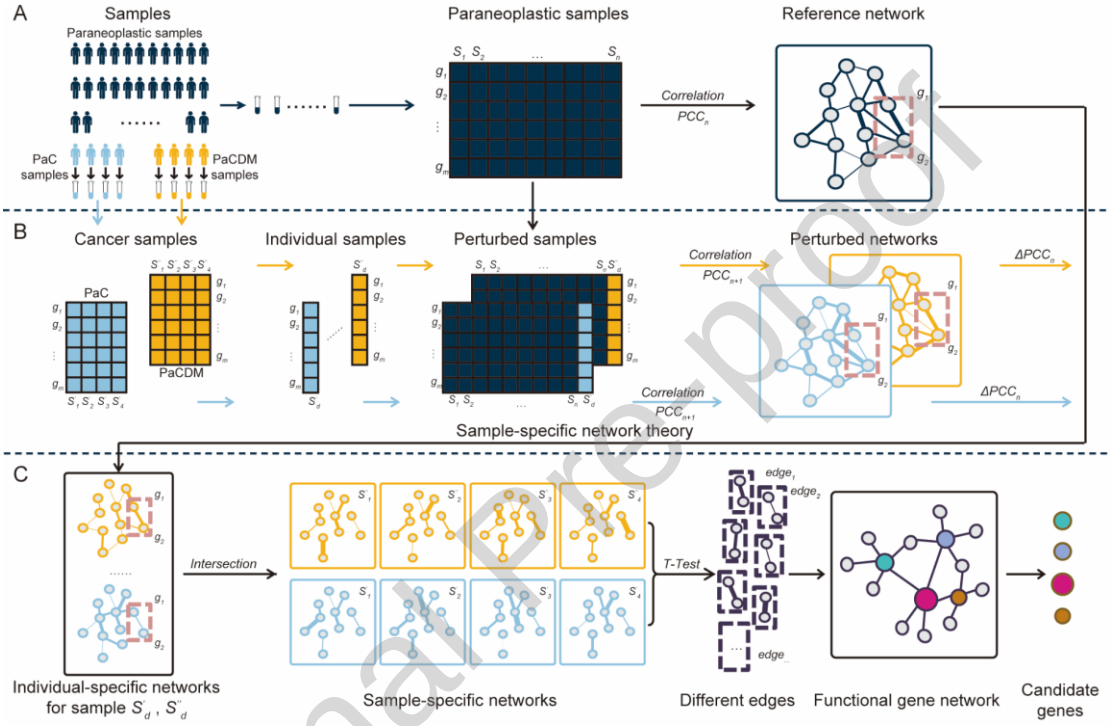
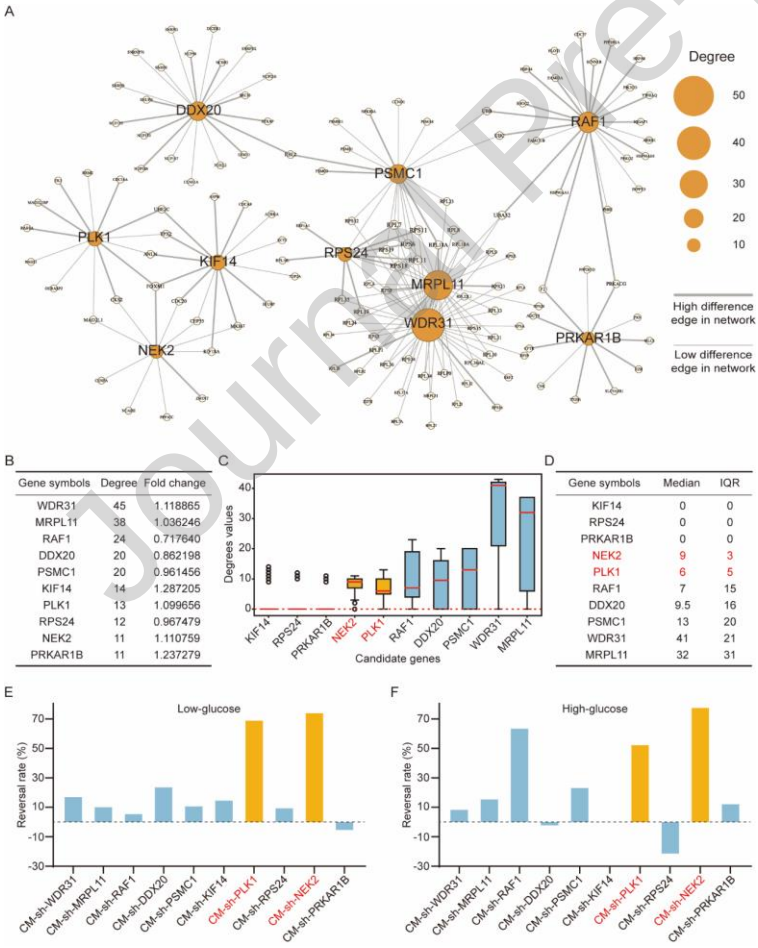


Fig. 1 Flowchart for constructing a functional gene network of pancreatic cancer-associated diabetes mellitus. (A) A reference network can be constructed by the correlations between genes based on expression data of paraneoplastic samples (*n* samples, *m* genes/sample), i.e. computing the PCC_n (the Pearson correlation coefficient (*PCC*) of an edge in the reference network with *n* samples) of each pair of genes as an edge in the network. PaC, pancreatic cancer without diabetes mellitus (DM). PaCDM, pancreatic cancer with DM. (B) A new sample S'_d from PaC samples and a new sample S''_d from PaCDM samples are added to reference samples to form two types of perturbed samples, respectively, and two types of perturbed networks with these additional samples are constructed in the same way by the correlation PCC_{n+1} of the corresponding combined data. (C)

Based on SSN theory, for each sample from PaC and PaCDM samples, the individual-specific network is constructed by the significant difference of the corresponding edge between the reference and perturbed networks in terms of *PCC*, i.e. $\Delta PCC_n = PCC_{n+1}\text{-}PCC_n$ for each edge. Two types (PaCDM and PaC) of SSNs are constructed by retained intersected edges of all corresponding individual-specific networks, and functional gene network of PaCDM is constituted by the significantly different edges between two types of SSNs.



Gene symbols	Degree	Fold change
WDR31	45	1.118865
MRPL11	38	1.036246
RAF1	24	0.717640
DDX20	20	0.862198
PSMC1	20	0.961456
KIF14	14	1.287205
PLK1	13	1.099656
RPS24	12	0.967479
NEK2	11	1.110759
PRKAR1B	11	1.237279

Gene symbols	Median	IQR
KIF14	0	0
RPS24	0	0
PRKAR1B	0	0
NEK2	9	3
PLK1	6	5
RAF1	7	15
DDX20	9.5	16
PSMC1	13	20
WDR31	41	21
MRPL11	32	31

Fig. 2 *NEK2* and *PLK1* may be potential driver genes of pancreatic cancer-associated diabetes

mellitus. (A) The functional gene subnetwork of pancreatic cancer-associated diabetes mellitus. The 10 candidate genes are highlighted as orange, and other nodes are the first-order neighbors (genes) with the top 10 candidate genes. The node size indicates the degree of individual genes, and the thickness of the edges represents the magnitude of the difference in the gene-gene correlation between the two types of cancer samples. The detailed differential network is provided in Fig. S1A. WDR31, WD repeat domain 31; MRPL11, Mitochondrial ribosomal protein L11; RAF1, Raf-1 proto-oncogene, serine/threonine kinase; DDX20, DEAD-box helicase 20; PSMC1, Proteasome 26S subunit, ATPase 1; KIF14, Kinesin family member 14; PLK1, Polo like kinase 1; RPS24, Ribosomal protein S24; NEK2, NIMA related kinase 2; PRKAR1B, Protein kinase cAMP-dependent type I regulatory subunit beta. (B) The basic information for the top 10 candidate genes. Gene symbols: the official symbol for each gene; Degree: the degree of each gene in the functional gene subnetwork (or the number of neighbors for each gene); Fold change: the ratio of PaCDM expression to PaC expression. (C-D) The box plot (C) and median and interquartile range (IQR) (D) of degree values of 10 candidate genes as top genes in the network with the adjustment of threshold of significantly different edge selection. All candidate genes are arranged from smallest to largest according to the IQR. (E-F) Reversal effects of 10 candidate genes knockdown in PANC1 cells on PANC1 cell-derived conditioned medium (CM)-induced decrease in insulin secretion in MIN6 cells under low-glucose (E) and high-glucose (F) stimulation by glucose stimulated insulin secretion test. The two most likely driver genes are highlighted in orange. Detailed results are provided in Fig. S2.

Journal Pre-proof

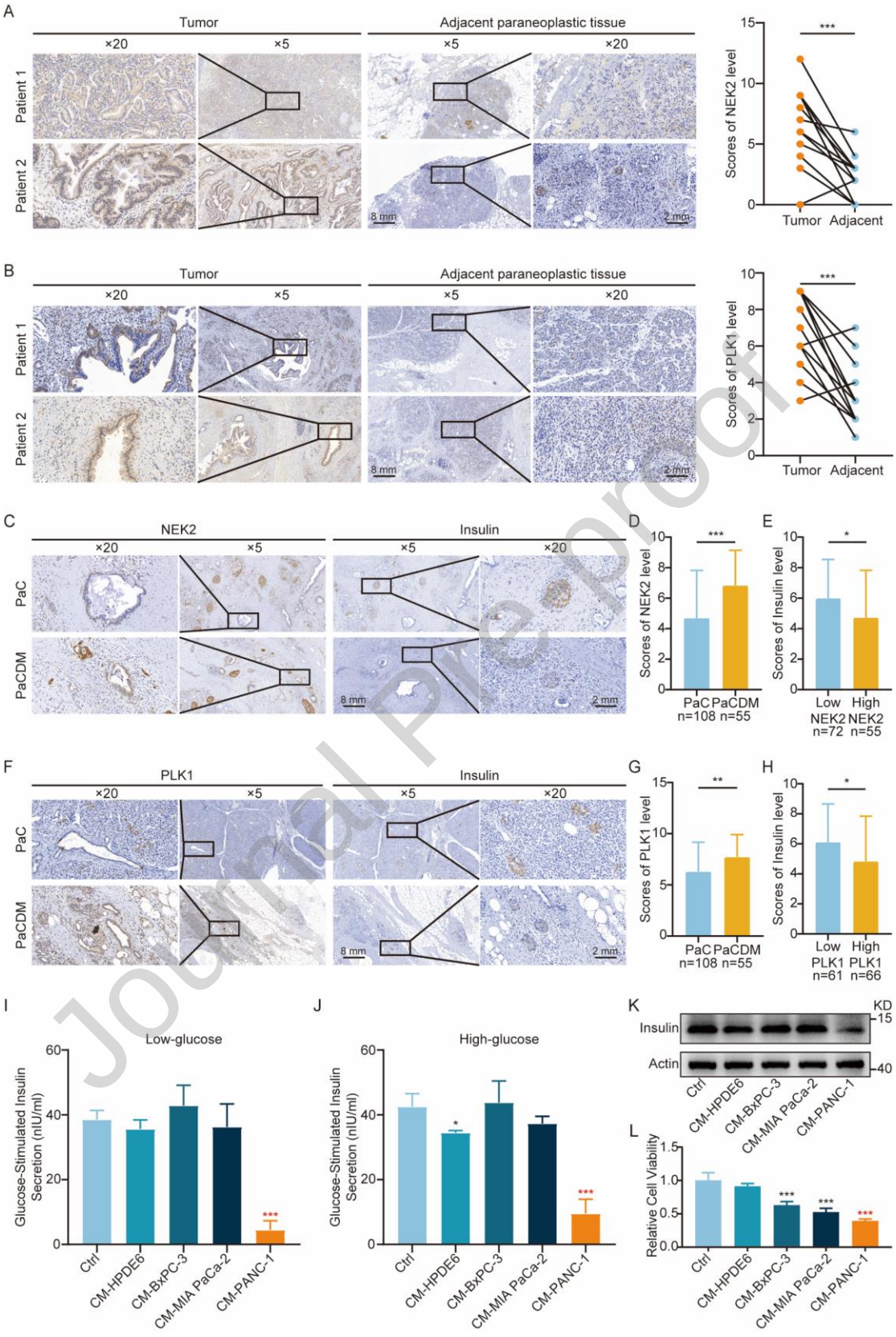


Fig. 3 NEK2 and PLK1 are upregulated in pancreatic cancer and are associated with the onset of PaCDM independently. (A-B) Representative images of NEK2 (A) and PLK1 (B) staining and

corresponding scores of NEK2 (A) and PLK1 (B) level in tumor tissues and adjacent paraneoplastic tissues from 15 patients with pancreatic cancer. (C-H) Representative images of NEK2 and Insulin staining in tumor tissues (C) and PLK1 and Insulin staining in tumor tissues (F) from patients with pure pancreatic cancer (PaC) and pancreatic cancer with diabetes mellitus (PaCDM). Comparison of scores of NEK2 (D) and PLK1 (G) level in pancreatic tumor tissues between patients in PaC (n=108) group and PaCDM (n=55) group. Comparison of scores of Insulin level between the high-NEK2 (score of NEK2 level ≥ 7) group (n=55) and the low-NEK2 (score of NEK2 level ≤ 6) group (n=72) (E) and between the high-PLK1 (score of PLK1 level ≥ 7) group (n=66) and the low-PLK1 (score of PLK1 level ≤ 6) group (n=61) (H), among 127 patients with Insulin scores available. (I-J) The difference of low (I) and high (J) glucose-stimulated insulin secretion (GSIS) levels between MIN6 cells treated with control medium (Ctrl) and CM collected from HPDE6 (CM-HPDE6) and 3 wild-type pancreatic cancer cell lines (BxPC-3 (CM-BxPC-3), MIA PaCa-2 (CM-MIA PaCa-2), PANC-1 (CM-PANC-1)) for 48 hours by a Mouse Insulin ELISA kit. (K) Insulin protein content in MIN6 cells treated with Ctrl, CM-HPDE6, CM-BxPC-3, CM-MIA PaCa-2, CM-PANC-1 for 48 hours by western blotting. (L) The cell viability of MIN6 cells treated with Ctrl, CM-HPDE6, CM-BxPC-3, CM-MIA PaCa-2, CM-PANC-1 for 72 hours by CCK-8 kit. For figures I-L, all experiments were repeated for three times. * $p < 0.05$; ** $p < 0.01$; *** $p < 0.001$. Student's t-test analysis was used for comparison between two groups.

Journal Pre-proof

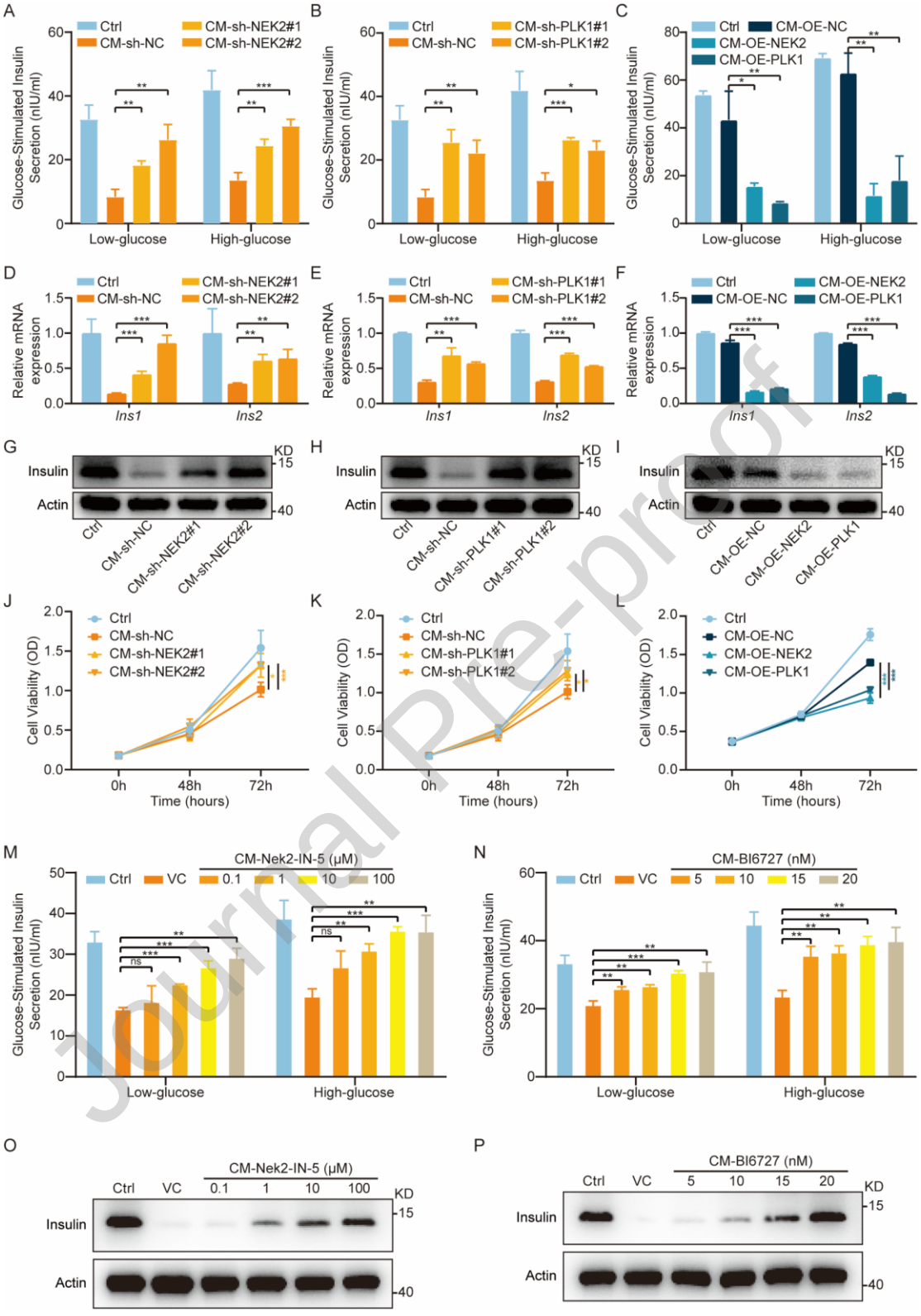


Fig. 4 NEK2 and PLK1 may cause pancreatic cancer cell-induced dysfunction of insulin secretion and inhibition of cell viability in MIN6 cells. (A-B) The difference of low and high GSIS levels between MIN6 cells treated with Ctrl, CM collected from sh-NC-transfected PANC-1 cells (CM-

sh-NC) and PANC-1 cells pretreated with knockdown of NEK2 (CM-sh-NEK2#1/#2, A) or PLK1 (CM-sh-PLK1#1/#2, B) for 48 hours by a Mouse Insulin ELISA kit. (C) The difference of low-glucose and high-glucose GSIS levels between MIN6 cells treated with Ctrl, CM collected from OE-NC-transfected MIA PaCa-2 cells (CM-OE-NC) and MIA PaCa-2 cells pretreated with overexpression of NEK2 (CM-OE-NEK2) or PLK1 (CM-OE-PLK1) for 48 hours by a Mouse Insulin ELISA kit. (D-E) The different relative mRNA expression levels of *Ins1* and *Ins2* in MIN6 cells treated with Ctrl, CM-sh-NC and CM-sh-NEK2#1/#2 (D) or CM-sh-PLK1#1/#2 (E) for 48 hours by qRT-PCR. (F) The different relative mRNA expression levels of *Ins1* and *Ins2* in MIN6 cells treated with Ctrl, CM-OE-NC, CM-OE-NEK2 and CM-OE-PLK1 for 48 hours by qRT-PCR. (G-H) The different insulin content in MIN6 cells treated with Ctrl, CM-sh-NC and CM-sh-NEK2#1/#2 (G) or CM-sh-PLK1#1/#2 (H) for 48 hours by western blotting. (I) The different insulin content in MIN6 cells treated with Ctrl, CM-OE-NC, CM-OE-NEK2 and CM-OE-PLK1 for 48 hours by western blotting. For figures D-F, the *Ins1* and *Ins2* mRNA expression level of Ctrl group served as corresponding reference (set at 1). (J-K) Detection of cell viability of MIN6 cells treated with Ctrl, CM-sh-NC and CM-sh-NEK2#1/#2 (J) or CM-sh-PLK1#1/#2 (K) after 0 h, 48 h, 72 h treatment by CCK8 kit. (L) Detection of cell viability of MIN6 cells treated with Ctrl, CM-OE-NC, CM-OE-NEK2 and CM-OE-PLK1 after 0 h, 48 h, 72 h treatment by CCK8 kit. (M-P) The difference of low and high glucose-stimulated GSIS levels (M-N) and insulin content (O-P) between MIN6 cells treated with Ctrl, CM-sh-NC and CM derived from PANC-1 cells pretreated with increasing concentrations of the NEK2 inhibitor Nek2-IN-5 (0, 0.1, 1, 10, and 100 μM) (CM-Nek2-IN-5, M and O) and the PLK1 inhibitor BI6727 (0, 5, 10, 15, and 20 nM) (CM-BI6727, N and P) for 48 hours by a Mouse Insulin ELISA kit and western blotting. VC, Vehicle control. All experiments

Journal Pre-proof

were independently repeated three times. * $p < 0.05$; ** $p < 0.01$; *** $p < 0.001$. Student's t-test analysis was used for comparison between two groups.

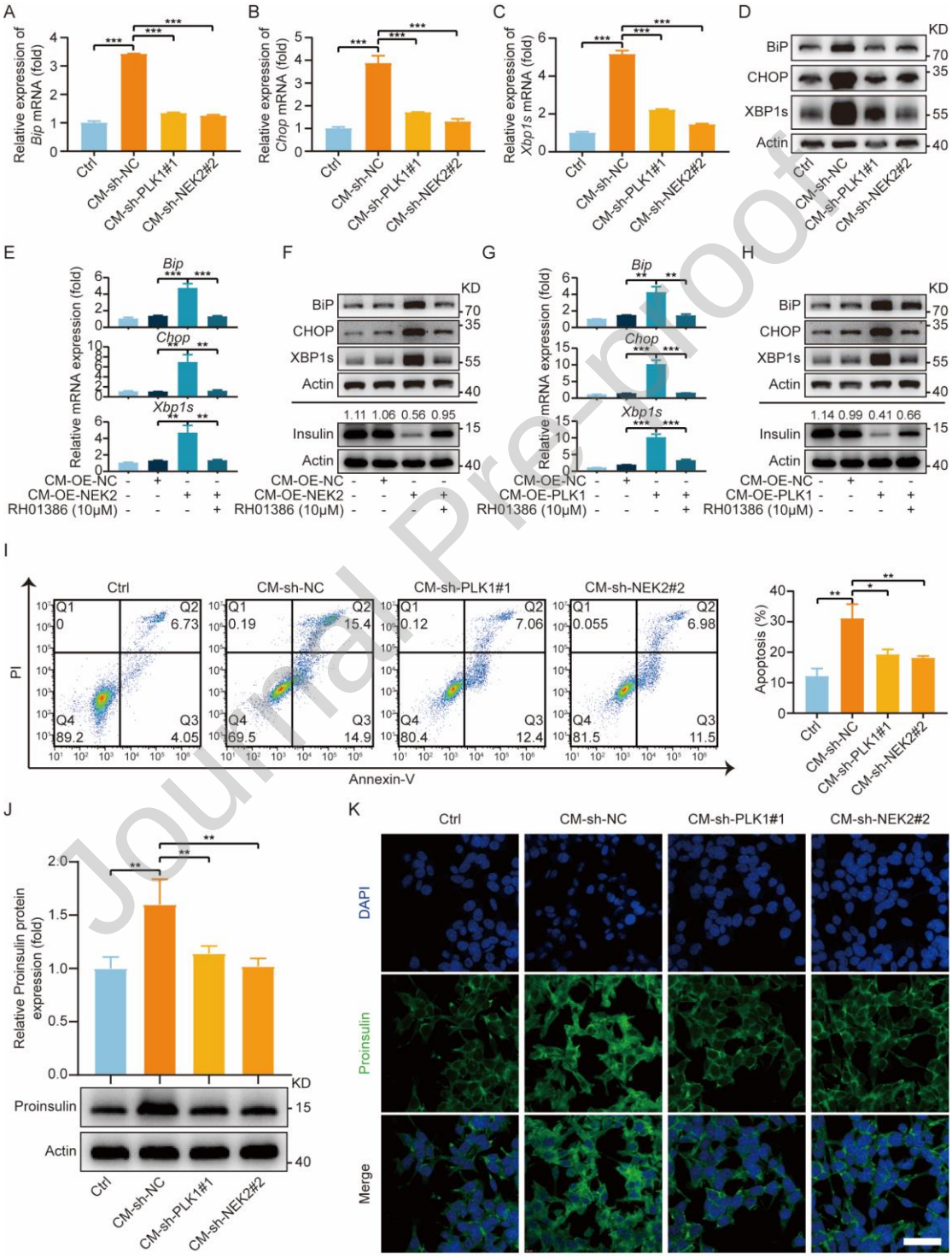
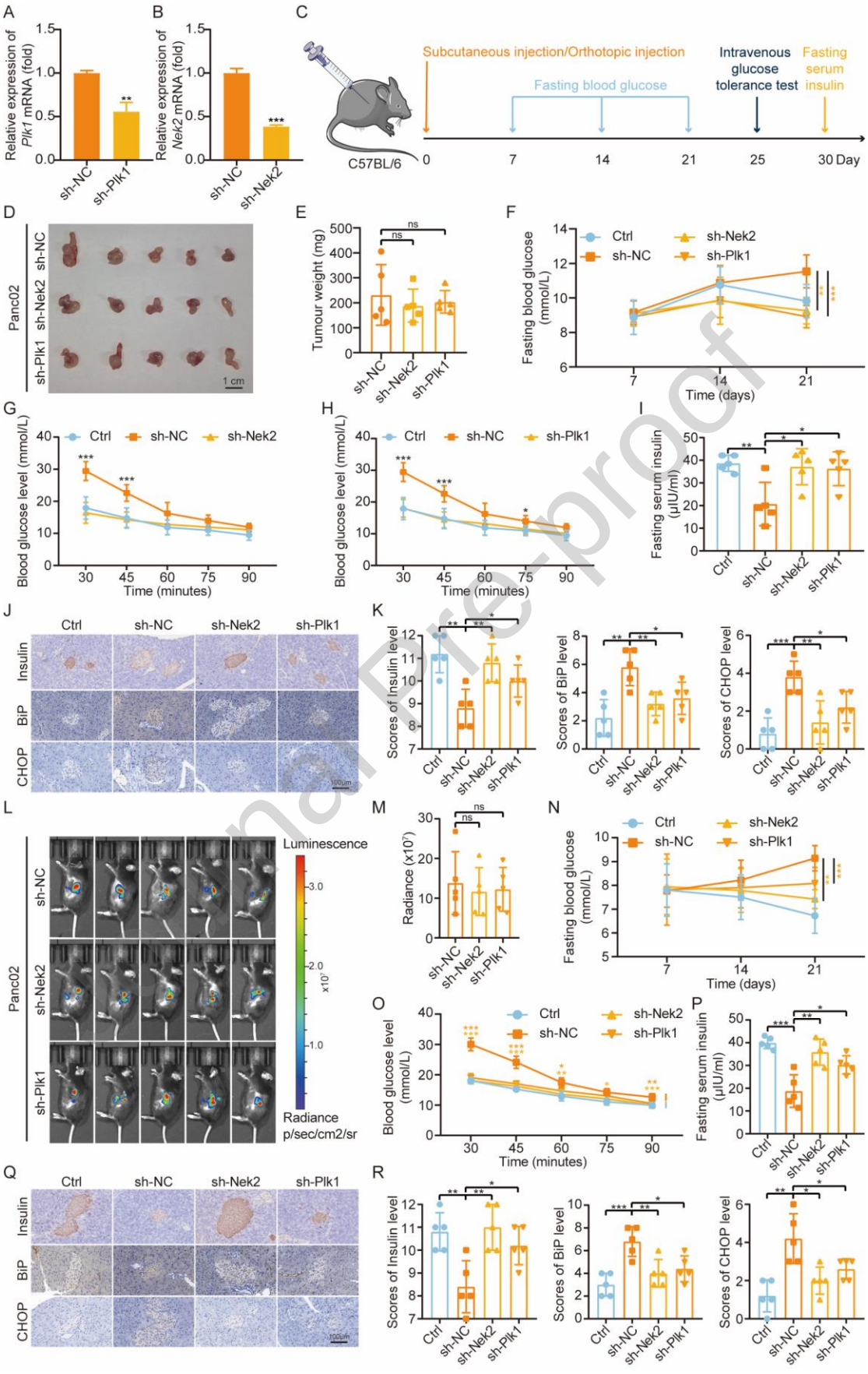


Fig. 5 NEK2 and PLK1 may cause PaC cell-induced dysfunction by inducing endoplasmic

reticulum stress in MIN6 cells. (A-C) The mRNA levels of markers (*Bip* (A), *Chop* (B) and *Xbp1s* (C)) of endoplasmic reticulum (ER) stress in MIN6 cells treated with Ctrl and CM-sh-NC, CM-sh-PLK1#1 and CM-sh-NEK2#2 for 48 hours by qRT-PCR. The mRNA expression level of Ctrl group served as corresponding reference (set at 1). (D) The protein levels of markers of ER stress (BiP, CHOP and XBP1s) in MIN6 cells treated with Ctrl, CM-sh-NC, CM-sh-PLK1#1 and CM-sh-NEK2#2 for 48 hours by immunoblotting. (E-F) The relative mRNA expression levels (E) and protein level (F) of ER stress markers and insulin content (F) in MIN6 cells treated with Ctrl, CM-OE-NC and CM-OE-NEK2 and CM-OE-NEK2+RH01386 (10 μM) for 48 hours by qRT-PCR and western blotting. (G-H) The relative mRNA expression levels (G) and protein level (H) of ER stress markers and insulin content (H) in MIN6 cells treated with Ctrl, CM-OE-NC, CM-OE-PLK1 and CM-OE-PLK1+RH01386 (10 μM) for 48 hours by qRT-PCR and western blotting. For figures E, G, the mRNA expression level of Ctrl group served as corresponding reference (set at 1). For figures F, H, the ratios of Insulin/Actin grayscale values are indicated above the corresponding bands to provide a quantitative representation of Insulin expression relative to Actin. Actin serves as the internal reference to normalize Insulin expression levels. (I) The representative images of apoptosis flow cytometry analysis and the percentage of apoptosis cells of MIN6 cells treated with Ctrl, CM-sh-NC, CM-sh-PLK1#1 and CM-sh-NEK2#2 for 48 hours by flow cytometry. (J) The relative proinsulin protein levels and proinsulin content in MIN6 cells treated with Ctrl, CM-sh-NC, CM-sh-PLK1#1 and CM-sh-NEK2#2 for 48 hours by immunoblotting. The proinsulin protein level of Ctrl group served as reference (set as 1). (K) Fluorescence immunocytochemistry of proinsulin in MIN6 cells treated with Ctrl, CM-sh-NC, CM-sh-PLK1#1 and CM-sh-NEK2#2 for 48 hours. Cells were stained with an anti-proinsulin antibody followed by a Cy3-conjugated secondary antibody,

and the proinsulin signal is displayed in green pseudocolor; DAPI is shown in blue. White scale bar, 50 μm. All experiments were independently repeated three times. * $p < 0.05$; ** $p < 0.01$; *** $p < 0.001$. Student's t-test analysis was used for comparison between two groups.

Journal Pre-proof



Journal Pre-proof

Fig. 6 Silencing *NEK2* and *PLK1* in PaC cells may alleviate PaC cells-induced glucose intolerance *in vivo*. (A-B) Detection of knockdown efficiency of *Plk1* (A) and *Nek2* (B) in Panc02 cells by qRT-PCR. The mRNA expression level of sh-NC group served as corresponding reference (set at 1). (C) Flowchart illustrating the subcutaneous/orthotopic injection and experimental design of glucose tolerance *in vivo*. Four groups of mice were injected subcutaneously (D-K) or orthotopically (L-R) with Panc02 cells (Ctrl group: injected with DMEM medium; sh-NC group: injected with Panc02 cells pretreated with sh-NC; sh-Nek2 group: injected with Panc02 cells pretreated with sh-Nek2; sh-Plk1 group: injected with Panc02 cells pretreated with sh-Plk1, n=5 per group). Mice received weekly fasting blood glucose for consecutive three weeks after subcutaneous/orthotopic injection. Intravenous glucose tolerance test was conducted at twenty-five days after subcutaneous injection, and finally fasting serum insulin level was measured at thirty days after subcutaneous/orthotopic injection. (D, L) Images of subcutaneous tumors formed (n=5 per group, D) and bioluminescence imaging visualizing the growth of orthotopic xenografts formed (n=5 per group, L) of mice in sh-NC group, sh-Nek2 group and sh-Plk1 group. (E, M) Tumor weights of subcutaneous tumors (E) and average radiance from the pancreas area (M) of mice in sh-NC group (n=5), sh-Nek2 group (n=5) and sh-Plk1 group (n=5). Tumor weights and average radiance are expressed as the mean ± SD of fifteen mice, respectively. (F, N) The fasting blood glucose levels of mice were measured in four groups of mice at 7, 14, and 21 days after subcutaneous injection (F) or orthotopic injection (N). Data represent the mean ± standard deviation for each group at each time point. (G-H, O) The intravenous glucose tolerance tests were performed in C57BL/6 mice (n = 5 per group) from the Ctrl, sh-NC, and sh-Nek2 groups (G) and the sh-Plk1 group (H) after subcutaneous injection, and in the corresponding groups after orthotopic injection (O). Mice were subjected to intravenous

glucose tolerance tests, and blood glucose levels were measured using a glucometer at 30, 45, 60, 75, 90 minutes after injection of 5% glucose solution. (I, P) The fasting serum insulin levels were measured in four groups of C57BL/6 mice (n = 5 per group) that received subcutaneous (I) or orthotopic (P) injection, using a mouse insulin ELISA kit. (J-K, Q-R) Representative images of IHC staining (J, Q) and IHC score (K, R) of Insulin and ER stress markers (BiP and CHOP) in pancreases from C57BL/6 mice by subcutaneous (J-K) and orthotopic (Q-R) injection. * $p < 0.05$; ** $p < 0.01$; *** $p < 0.001$; ns: non significance. Student's t-test analysis was used for comparison between two groups.

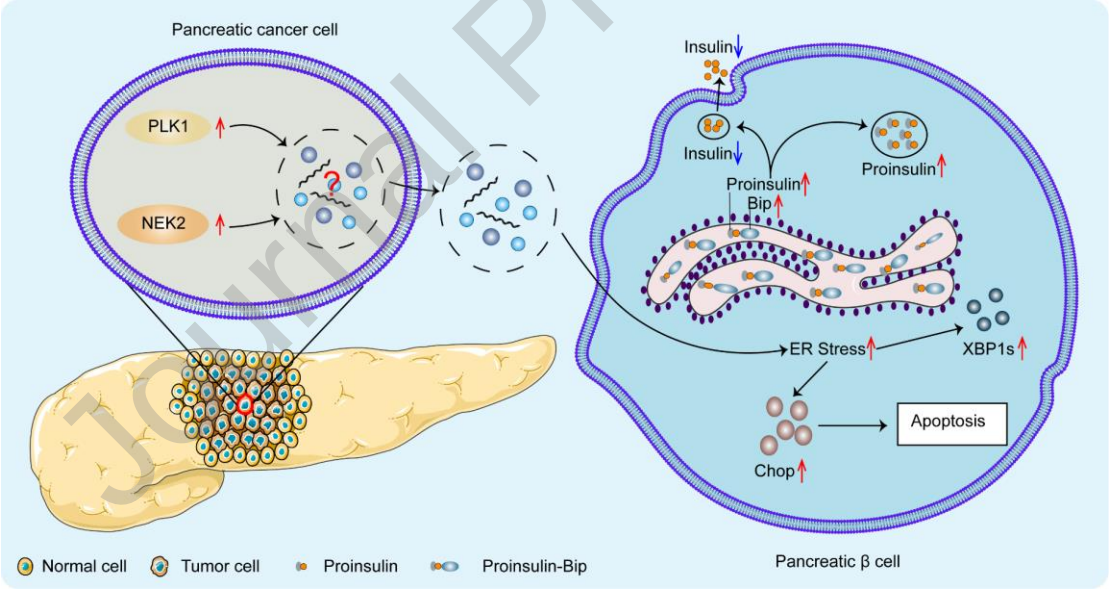


Fig. 7 Proposed mechanism of NEK2- and PLK1-dominated pancreatic cancer cell-induced dysfunction of pancreatic β cell. NEK2 and PLK1 over-expressed in pancreatic cancer cells induce ER stress and inhibit proinsulin processing in the ER in β cells. This leads to the accumulation of proinsulin and the decrease of insulin protein content, thereby inhibiting insulin secretion by

pancreatic β cells. Activated *Chop* can induce apoptosis of pancreatic β cells, thereby inhibiting cell viability. However, the effector molecules, that mediates pancreatic cancer cells-induced damage to pancreatic β cells, is unknown.

Additional files

Additional file 1: Supplemental Tables and Figures

Data Supplement: 1. Table S1; 2. Table S2; 3. Table S3; 4. Table S4; 5. Table S5; 6. Figure S1; 7. Figure S2; 8. Figure S3; 9. Figure S4

Additional file 2: Raw image files of Western blotting

Original western blots

Additional file 3: The meaning of all symbols (e.g. rxy, n, d) in Equation 1-3

The detail explanation of the meaning of all symbols (e.g. rxy, n, d) in Equation 1-3

Additional file 4: The melting curves for each pair of primers

The melting curves for each pair of primers

Additional file 5: The emission spectrum of green channel

The emission spectrum of green channel (anti-Proinsulin antibody)

Journal Pre-proof

Declaration of interests

☒ The authors declare that they have no known competing financial interests or personal relationships that could have appeared to influence the work reported in this paper.

☐ The authors declare the following financial interests/personal relationships which may be considered as potential competing interests:

Journal Pre-proof